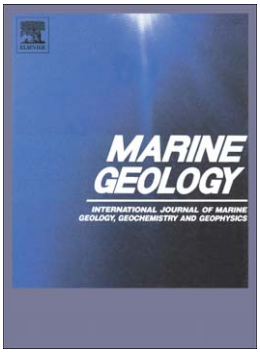

Sedimentological and paleoenvironmental scenario before, during, and after the Messinian Salinity Crisis: The San Miguel de Salinas composite section (western Mediterranean)

Hugo Corbí, Jesús M. Soria, Carlos Lancis, Alice Giannetti, José E. Tent-Manclús, Jaume Dinarès-Turell

PII: S0025-3227(16)30099-8
DOI: doi: 10.1016/j.margeo.2016.05.017
Reference: MARGO 5471

To appear in: *Marine Geology*

Received date: 15 July 2015
Revised date: 20 May 2016
Accepted date: 25 May 2016

Please cite this article as: Corbí, Hugo, Soria, Jesús M., Lancis, Carlos, Giannetti, Alice, Tent-Manclús, José E., Dinarès-Turell, Jaume, Sedimentological and paleoenvironmental scenario before, during, and after the Messinian Salinity Crisis: The San Miguel de Salinas composite section (western Mediterranean), *Marine Geology* (2016), doi: 10.1016/j.margeo.2016.05.017

Sedimentological and paleoenvironmental scenario before, during, and after the Messinian Salinity Crisis: The San Miguel de Salinas composite section (western Mediterranean)

Highlights

1) The sedimentary record is divided into three synthems: Messinian I (pre-evaporitic), Messinian II (syn-evaporitic), and Pliocene (post-evaporitic).

2) Marls associated with gypsum beds (syn-evaporitic phase) record dwarf planktonic foraminifera.

3) The syn-evaporitic phase (chron 3Cr) records major changes in water salinity in a stressed marine environment.

4) Two erosional surfaces correspond to the intra- and end-Messinian unconformities.

5) The end-Messinian unconformity is represented by an incised paleovalley.

Hugo Corbí[1*], Jesús M. Soria[1], Carlos Lancis[1], Alice Giannetti[1], José E. Tent-Manclús[1], Jaume Dinarès-Turell[2]

[1] Department of Earth Sciences and the Environment, University of Alicante, Apdo. Correos 99, San Vicente del Raspeig, 03080 Alicante, Spain.

[2] Istituto Nazionale di Geofisica e Vulcanologia, Via di Vigna Murata, 605, 00143 Rome, Italy.

*Corresponding author: hugo.corbi@ua.es

Abstract

A composite stratigraphic section ranging from the Messinian to the Pliocene, recording the most important phases of the Messinian Salinity Crisis, is represented in the San Miguel de Salinas area (Bajo Segura basin, SE Spain). Detailed magnetostratigraphic and facies analyses and foraminifer and nannoplankton assemblage studies were carried out. Integration of the

results has allowed the characterization of the pre-evaporitic (synthem Messinian I), syn-evaporitic (synthem Messinian II), and post-evaporitic phases (synthem Pliocene) from a paleoenvironmental and chronostratigraphic standpoint. The pre-evaporitic phase is late Messinian and records a shallowing-upward trend. The syn-evaporitic phase took place in chron C3r and is characterized by laminated marls with intercalated selenitic gypsum beds and sandstones. Variations in foraminifer and nannoplankton assemblages together with episodic gypsum precipitation record major changes in water salinity in a stressed marine environment. The pre- and syn-evaporitic phases are separated by the intra-Messinian unconformity, represented by an erosional surface related with a sea-level fall. After the evaporitic phase, a sea-level fall generates the end-Messinian unconformity, whose strongly erosional nature is evidenced by the deeply carved paleovalley of San Miguel de Salinas. The post-evaporitic phase begins in the earliest Pliocene and records the re-establishment of normal marine conditions in the basin. Since the San Miguel de Salinas composite section can be considered as a benchmark for the study of the evolution of marginal Mediterranean basins during the Messinian Salinity Crisis, the detailed characterization of these different phases is of great importance in understanding this event.

Key-words: Messinian Salinity Crisis; Mediterranean, Betic Cordillera, Bajo Segura basin; paleoenvironment; chronostratigraphy

1. Introduction

The Messinian Salinity Crisis (MSC) has been considered one of the most unique events in the history of the Mediterranean. The discovery of the Messinian evaporites in the center of the Mediterranean Sea, and especially the formulation of the deep-basin desiccation hypothesis (Hsü et al., 1977, 1973), has attracted increasing attention over the years. The complete Messinian evaporitic suite at the center of the Mediterranean has been recognized in seismic profiles (Montadert et al., 1978), but is poorly documented because only its uppermost part

has been drilled. Nevertheless, the MSC can be studied from the Messinian evaporites cropping out in marginal basins of the eastern Betic Cordillera, fairly close to the Mediterranean (e.g. Sorbas, Almería-Nijar and Bajo Segura basins; e.g. Martín and Braga, 1994; Riding et al., 1999, 1998; Krijgsman et al., 2001; Braga et al., 2006; Lu et al., 2006; Soria et al., 2008a, 2008b; Caracuel et al., 2011) and in the tectonically uplifted portions (i.e. Sicily; Hilgen and Krijgsman, 1999; Roveri et al., 2008). In fact, the Late Miocene evaporites deposited prior to the MSC in the three interior basins of the Betic Cordillera (Granada, Lorca, and Fortuna) reflect the late-Tortonian marine restriction of the Betic seaway (the marine connection between the Atlantic and the Mediterranean) (e.g. Krijgsman et al., 2000; Corbí et al., 2012).

After more than forty years of studies mostly based on onshore sections, the Messinian Salinity Crisis debate continues, focusing mainly on the nature of the evaporites (deep vs shallow Mediterranean basin) and timing of the evaporitic deposition (synchronous vs diachronous). Roveri et al. (2014), Rouchy and Caruso (2006), Braga et al. (2006) and Clauzon et al. (1996) propose synthetic models that combine the onshore and offshore record into a single unified scenario. In the proposed models, the chronology, paleoenvironmental changes, and distribution of the main evaporitic stages, as well as the position of the Messinian erosional surfaces are discussed. In the Mediterranean margins, the stratigraphic location of the main erosional surface has been subject to opposing interpretations, mainly due to the problems of correlation between the central and marginal evaporites (see Riding et al., 1998, 1999, 2000; Fortuin et al., 2000; Krijgsman et al., 2001; Braga et al., 2006; Soria et al., 2008a, 2008b; Roveri et al., 2009; Manzi et al., 2013).

The San Miguel de Salinas composite section (hereafter SMdS) is located in the Betic margin of the western Mediterranean and ranges from the late Messinian to early Pliocene (Montenat, 1990). Its importance derives from being the Messinian evaporite outcrop nearest to the Mediterranean in the Bajo Segura basin and recording the different phases of the salinity crisis.

This section includes the pre-, syn-, and post-evaporitic units, with two main features: (1) the record of a single evaporitic unit dominated by gypsum, without halite or potassium salts, and (2) the existence of two major unconformities (erosional surfaces), located at the base and top of the evaporitic unit. All the studied stratigraphic units of the SMdS section were deposited under marine conditions; therefore, this section can be considered ideal for the study of planktonic and benthic foraminifera and calcareous nannoplankton to assess the paleoenvironmental conditions throughout the Messinian and Pliocene. Moreover, the very good exposure of the outcrops allows a detailed analysis of the stratigraphic architecture and the sedimentary facies, key tools for the reconstruction of the depositional environments. Furthermore, detailed biostratigraphic (planktonic foraminifera and calcareous nannoplankton) and magnetostratigraphic data have opened up the possibility of proposing a chronostratigraphic framework for the studied deposits. In short, our work shows that the SMdS composite section reveals key features that help to understand the complex Messinian paleoenvironmental evolution in the peri-Mediterranean marginal basins in SE Spain.

2. The Bajo Segura basin: Geological and stratigraphic setting

The study area belongs to the Bajo Segura basin, a Mediterranean marginal basin of the eastern Betic Cordillera (Fig. 1A-B). The basin's sedimentary infill seals the contact between the two major geological domains in this mountain range: the External Zone (or South Iberian Paleomargin) to the north and the Internal Zone (or Alboran Block) to the south. The Bajo Segura basin was paleogeographically established in the late Miocene after the orogenic movements that caused the collision of the Alboran Block (Internal Zone) against the South-Iberian Paleomargin (External Zone) (Soria et al., 2008b). The southern part of the basin, where our work focuses (Fig. 1C), has one of the most complete Messinian and Pliocene records of the Mediterranean margins as regards both the variety of depositional environments and the time range (Soria et al., 2005, 2008a, 2008b, 2014; Caracuel et al., 2011, 2004; Krijgsman et al.,

2006; Corbí, 2010; García-García et al., 2011).

According to the most recent studies (Soria et al., 2008a, 2008b), the marine Messinian to Pliocene sedimentary record of the Bajo Segura basin can be divided into three major allostratigraphic units (synthems), termed Messinian I (MI), Messinian II (MII), and Pliocene (P). These synthems are bounded by two basin-wide unconformities: the intra-Messinian unconformity (i-M) and the end-Messinian one (e-M) (Fig. 2A). Synthem MI is formed by four correlative depositional systems (*sensu* Fisher and McGowen, 1967) that, from the proximal to the distal one, are: (a) red clays with paleosols and channel-like conglomerate beds, corresponding to alluvial fans; (b) marls and marly limestones with frequent macro- and microvertebrate sites, deposited in a palustrine setting; (c) sandstones and reefal limestones typical of coastal and shelf environments; and (d) gray and brownish plankton-rich marls, cyclically arranged, with sandy turbiditic beds and slumps, interpreted as slope and pelagic basin deposits. Synthem MII overlies the intra-Messinian unconformity, which is represented by an erosional surface with subaerial exposure features. This synthem is composed of four depositional systems that, from the most proximal to the most distal one, are: (a) alluvial red clays; (b) palustrine marls and limestones, passing distally to coastal deposits, which include lagoonal marls, supratidal stromatolites, and beach oolitic grainstones; (c) shallow-marine sandstones and marls; and (d) shallow-marine evaporites interbedded with laminated marls. The top of this synthem coincides with the end-Messinian unconformity, represented by an erosional surface, which shows deep incised paleovalleys (Soria et al., 2008a, 2008b) filled by synthem P sediments. In synthem P, four depositional systems can be differentiated: (a) coastal and shallow marine conglomerates that fill the aforementioned paleovalleys; (b) marine marls; (c) coastal and shallow marine sandstones; and (d) alluvial clays and conglomerates. The three synthems (MI, MII, and P) record high sea-level sedimentary phases when the sea occupied the Bajo Segura basin (Soria et al., 2008a, 2008b). The two unconformities (intra- and end-Messinian) mark two erosional periods in the basin produced

by two major sea-level falls.

3. Materials and Methods

The SMdS composite section was constructed by joining the sections of Lo Rufete, Km16, and Canal, all located near the town of San Miguel de Salinas (Fig. 2B). The Lo Rufete section is north of the Torremendo-San Miguel de Salinas road (CV-951), near the Lo Rufete Lakeview Mansions estate. The Km16 section is the classic section of Shearman and Ortí-Cabo (1976), Ortí-Cabo and Shearman (1977), Montenat (1990), Michalzik et al. (1993), Rosell et al. (1994), Michalzik (1996), Playà et al. (2000), Soria et al. (2008b), and Corbí (2010) starting at the 16 kilometer marker of the Orihuela-San Miguel de Salinas road (CV-95). The Canal is the section of the Tajo-Segura water transfer canal, located west of the town of San Miguel de Salinas. In all three sections, the beds dip between 10° to 20° to the east.

Fifty-four samples were collected from the Lo Rufete, Km16, and Canal sections to study foraminifer assemblages (Fig. 3A and B). Each sample was wet-sieved to collect the >125 µm fraction, identifying and counting around 300 specimens for the quantitative analysis. From a selection of 32 samples, the calcareous nannofossils were studied after preparing four smear slides for each sample following the centrifugation-sonication procedure described in Lancis et al. (2010). The smear slides were semiquantitatively analyzed under the 100x lens, scanning the whole slide to find all the biostratigraphic markers. To count the small placoliths, mean values were calculated using the percentage of those coccoliths found in 10 visual fields numbering around 3,000 nannoliths. Finally, the percentage of *Reticulofenestra pseudoumbilicus* >7 µm was determined after counting 500 nannoliths larger than 3 mm.

Regarding foraminifer analysis, we have considered the following variables: (1) abundance of selected benthic foraminifer paleoecological markers related to total number of benthic foraminifera per sample (A) considering the following ranges: occasional presence (A < 5%), common presence (6 %< A <20%), abundant (21%< A <50%), and dominant (>50%). (2)

Planktonic and benthic foraminifer diversity indices (taking into account the number of species per sample of each group separately) measured by H(s) (Shannon–Weaver, 1949) and species richness. (3) The percentage of planktonic foraminifera versus the total amount of foraminifera (%P), related to bathymetry (Wright, 1978; Van der Zwaan *et al*., 1990). And (4) the abundance ratio between warm-oligotrophic water planktonic foraminifera (mainly *Globigerinoides* spp., *Orbulina* spp., *Globoturborotalita apertura*) and cold-eutrophic planktonic species (*Globigerina bulloides*, *Turborotalita quinqueloba*, *Globigerinita glutinata,* and *Neogloboquadrina* spp.) (Sierro et al., 1999, 2003). This ratio varies from 0% (cold-eutrophic planktonic foraminifer dominance) to 100% (warm-oligotrophic planktonic foraminifer dominance). The paleoenvironmental interpretation of benthic foraminifer assemblages is based mainly on ecological data from Murray (1991) and other specific references cited in the text.

For the nannoplankton analysis, we examined the following variables: (1) the percentage of asteroliths, whose abundance is indicative of open marine conditions (Haq et al., 1980; Driever, 1988; Young, 1994; Lancis, 1998). (2) The percentage of dwarf asteroliths, whose abundance is indicative of restricted marine conditions (Müller, 1978, 1990; Lancis, 1998). (3) The number of *Reticulofenestra pseudoumbilicus* (>7 µm). (4) The number of *Reticulofenestra pseudoumbilicus* (5–7 µm) (the abundance of *Reticulofenestra pseudoumbilicus* of >7 µm is related to open marine conditions, whereas 5–7 µm forms are indicative of somewhat more restricted marine conditions) (Haq et al, 1980; Driever, 1988; Young, 1994; Lancis, 1998). (5) The number of small placoliths (including *Reticulofenestra minuta* and *Dictyococites productus)* as these r-strategist forms are indicators of nutrient-rich conditions (Aubry, 1992; Lancis, 1998; Wade and Bown, 2006). Consequently, they dominate in continental margin marine environments (Haq, 1980), which can suffer rapid and periodic eutrophication due to continental runoff and/or river input or nutrient supply due to upwellings.

The paleomagnetic study was based on a total of 35 unique sampling sites, comprising two

hand-samples at each site along the three sections (Fig. 3C and 4). Hand-samples were oriented in situ with a compass, and standard cubic specimens were later cut in the laboratory for analysis. Natural remanent magnetization (NRM) and remanence through demagnetization were measured on a 2G Enterprises DC SQUID high-resolution pass-through cryogenic magnetometer (manufacturer's noise level of 10–12 Am2) operated in a shielded room at the Istituto Nazionale di Geofisica e Vulcanologia (Rome, Italy). A Pyrox oven in the shielded room was used for thermal demagnetization, and alternating field (AF) demagnetization was performed with three orthogonal coils installed inline with the cryogenic magnetometer. Progressive stepwise AF demagnetization was routinely used and applied after a single heating step to 150°C. AF demagnetization included 14 steps (4, 8, 13, 17, 21, 25, 30, 35, 40, 45, 50, 60, 80, and 100 mT). Characteristic remanent magnetizations (ChRM) were computed by least-squares fitting (Kirschvink, 1980) on the orthogonal demagnetization plots (Zijderveld, 1967). The ChRM declination and inclination were used to derive the latitude of the virtual geomagnetic pole (VGP) of each sample. This parameter was taken as an indicator of the original magnetic polarity, normal polarity being indicated by positive VGP latitudes and reverse polarity by negative VGP latitudes.

4. Stratigraphy and Sedimentology

4.1. Stratigraphic framework

A synthetic stratigraphic framework (Fig. 3A) was reconstructed from the three study sections (Km16, Lo Rufete, and Canal), which have been selected since they contain the most significant features of the stratigraphic units described in this work. In this figure, synthem P3 of Soria et al. (2008a, 2008b) is not included since, although also represented in the area, it records continental environments (red clays and conglomerates) and hence is not pertinent to this work.

Following the terminology introduced by Soria et al. (2008b), the upper part of synthem MI and all of synthems MII and P crop out in the San Miguel de Salinas area (Fig. 2B). The three units share the presence of marine marls and shallow-water platform and coastal sandstones, whereas MIIa differs from all the other marl-dominated systems in that it contains selenite gypsum (Fig. 3B). Considering both the vertical evolution of depositional systems as well as the geometry of the sandstone lithosomes, synthems MI and MII seem to represent shallowing- and thickening-upward prograding megasequences (Fig. 3A and B). The prograding pattern in synthem MI has also been observed in other sections in the Bajo Segura basin (such as the Venta de la Virgen, Soria et al., 2014) and agrees with the stratigraphic model proposed by Montenat (1990). The depositional dip of the gypsum beds in depositional system MIIa matches the geometry of the clinoforms present in synthem MII (Fig. 3A), which also agrees with Montenat (1990).

The boundaries between the synthems are related to erosion and subaerial exposure. The boundary between synthems MI and MII is known as the intra-Messinian unconformity, and it is marked by a stromatolite level with metric-scale polygonal desiccation cracks, indicating an emersion phase (Fig.3B). The boundary between synthems MII and P represents the end-Messinian unconformity and shows typical erosional features such as the paleovalley in the San Miguel de Salinas area (Fig.3B). Correlative deeper and wider paleovalleys were documented in the Bajo Segura basin, the most important of which crops out in the La Pedrera section (Soria et al., 2008a, 2008b; García-García et al., 2011). As for sequence stratigraphy, synthems MI and MII correspond to highstand systems tracts and belong to incomplete depositional sequences since they are truncated at the top by discontinuities related to sea-level falls.

4.2. Sedimentary facies analysis and depositional interpretation

4.2.1. Synthem MI

This synthem is well exposed in the Lo Rufete section (Fig. 2B and 3) and was divided into two superimposed and gradational depositional systems (Fig. 5A): MIa (in the lower part) and MIb (in the upper part).

The MIa depositional system corresponds to a meter-thick alternation of gray marls and tobacco-colored (brownish) laminated marls, rich in foraminifera and calcareous nannoplankton (Fig. 5B). Although the precise definition of a sapropel (Kidd et al., 1978; Cramp and O'Sullivan, 1999) notes contents of more than 2% organic carbon, these brownish laminated layers can be considered sapropels or sapropelitic marls considering the less restrictive definition of Hilgen (1991), who described sapropels as "brownish, often laminated interbeds". These lithological pairs (gray and brownish marls) are equivalent to the cycles of the La Pedrera section (Soria et al., 2008a; Corbí, 2010) two kilometers north of the Lo Rufete section. This depositional system sporadically shows 5 to 20 cm-thick, fine-grained terrigenous sandstone beds with planar lamination (Fig. 5C). *Thalassinoides* are found in the upper part of the sandstone beds (Fig. 5D).

The MIb depositional system is made up of interbedded sandstones and sandy marls. It is 25 m thick in the Lo Rufete section and shows three thickening-upward sequences of terrigenous, fine- to coarse-grained sandstones (Fig. 5A). The most abundant constituents of the sandstones are quartz, feldspar, and carbonate lithoclasts, together with pectinids, ostreids, and other fragmented shallow-marine fossils. The sandy marl interbeds contain microfossils and nannofossils. The sandstone beds are intensively bioturbated and show hummocky and swaley cross-stratification (Fig. 5E and F), sometimes with rip-up mud clasts aligned with the internal lamination.

Based on the sedimentary analysis, the MI synthem is interpreted as a terrigenous shelf environment grading distally to a marly dominated pelagic marine basin. Note that, as shown in Figure 2A, in the southern part of the basin, in particular in Santa Pola Cape, synthem MI

records coral reefs (Soria et al., 2008a, 2008b) considered by Montenat (1990) to be a lateral equivalent to the La Virgen Formation (synthem MI of Soria et al., 2008a, 2008b). In the proximal part (MIb depositional system), sandy tempestites alternate with episodes of fair-weather muddy accumulation. The regular presence of hummocky and swaley cross-stratification indicates that these tempestites were deposited above the storm wave-base level by storm-ebb surges modeled by high-regime oscillatory flows (see similar models in Walker, 1979; Cheel, 1991; Brenchley et al., 1993). The regular alternation of tempestite beds and marls has been interpreted as precessional cycles in the neighboring section of Venta de la Virgen (Soria et al., 2014). According to these authors, the tempestite interval corresponds to insolation maxima/precession minima, whereas the marly interval represents insolation minima/precession maxima.

In the distal part (MIa depositional system), the gray marl/sapropelitic marl lithological pairs are equivalent to the cycles defined in the upper Abad Member of the Sorbas Basin (Krijgsman et al., 2001; Sierro et al., 2003). These cycles are ubiquitous throughout the Mediterranean basins prior to the Messinian Salinity Crisis (e.g. Betics, Apennines, Sicily, Greece, and Cyprus). Detailed cyclostratigraphic studies correlate the homogeneous marl/sapropel pairs with precessional orbital cycles (20–23 ka; Hilgen and Krijgsman, 1999; Krijgsman et al., 1999; Hüsing et al., 2009).

The intra-Messinian unconformity crops out exceptionally well in the Lo Rufete section, separating the MIb depositional system from the MII synthem. As stated above, it is marked by a two-meter-thick stromatolite bed formed by millimetric micrite laminae. This layer shows large polygonal desiccation cracks (Fig. 5 G—I), which cannot be interpreted as mud escape structures since the underlying levels comprise the coarse-grained sandstones of synthem MIb. These polygonal desiccation cracks indicate sudden shallowing with subsequent aerial exposure of the shallow-marine shelf represented by the MIb depositional system**.** In synthem

MII, marine marls with sandstone beds (MIIa system) overlie the stromatolite layer and hence the unconformity, indicating a return to marine conditions.

4.2.2. Synthem MII

In synthem MII, the lower depositional system (MIIa) is composed of marls alternating with sandstones and selenite gypsum, and the upper system (MIIb) is dominated by thickening-upward sandstone beds. Both depositional systems are best represented in the Km16 and Canal sections (Fig. 3 A and B).

The marls of the MIIa system are characterized by subtle lamination (Fig. 6A). The clear gray laminae correspond to sand, whereas the dark or black laminae correspond to sand-poor, sapropelitic sediments, with 1.5% total organic carbon (TOC). Planktonic and benthic foraminifera, calcareous nannoplankton, ostracods, siliceous sponge spicules, and well-preserved plant remains are present. The fine-grained sandstone levels have a thickness of 1–60 cm. The most common sedimentary structures are planar lamination, hummocky and swaley cross-stratification (Fig. 6B), and wave ripple cross-lamination (Fig. 6C). These sandstone beds lack fossil remains and trace fossils, which clearly differentiates them from the underlying MI system sandstones. The selenite gypsum of San Miguel de Salinas has been the subject of many detailed works (Shearman and Ortí-Cabo, 1976; Ortí-Cabo and Shearman, 1977; Montenat, 1990; Michalzik, 1996; Playà et al., 2000; Soria et al., 2008b; among others), with seven gypsum beds recognized (Ortí-Cabo and Shearman, 1977). The beds are labeled G1 to G7 (Fig. 6 D–H) and thickness ranges from 10 m for G1 to 80 centimeters for G7. Beds are tabular (Fig. 6E), in some cases changing laterally to cluster-like (*sensu* Michalzik, 1996) or supercone (*sensu* Dronkert, 1976) morphologies (Fig. 6G). Irregular bed tops and internal cavities filled with the laminated marls of the MIIa system are noteworthy (Fig. 6D). As mentioned by Michalzik (1996), fine detrital material with planktonic foraminifera and diatoms has been found between growth laminae of gypsum crystals. Concerning the selenite facies,

gypsum beds G1 to G5 are characterized by massive or giant selenite (Fig. 6F), whereas gypsum beds G6 and G7 are formed by branching selenite (Fig. 6H).

Depositional system MIIa changes upwards to thick sandstone beds interbedded with sandy marls, representing system MIIb. This system is characterized by (1) an increase in the number and thickness of the sandstone beds (see Km16 section in Fig. 3) and (2) the absence of gypsum beds. System MIIb evolved upwards from mixed carbonate-siliciclastic sandstones to carbonate-dominated oolitic grainstones. These carbonate-dominated facies were defined as a separate depositional system, called MIIb(o) (Fig. 3A and B) in reference to the high abundance of oolites.

The carbonate-siliciclastic mixed facies are organized in sequences made up of two intervals: the first one has planar lamination and rip-up mud clasts in the lower part of amalgamated sandstone beds, and an upper interval has hummocky and swaley cross-stratification (HCS) (Fig. 7A and B). Beds with HCS frequently show sediment deformation structures, described in nearby outcrops by Montenat (1990) and Alfaro et al. (2002). The carbonate facies present 2D and 3D sand waves, wave ripples with smooth crests (Fig. 7C), and low-angle or foreshore-type lamination. It is worth noting that these carbonate facies correspond to the Terminal Carbonate Complex defined by Esteban (1979). Similar oolitic grainstones have been described in other basins in SE Spain such as Almería-Níjar (Riding et al., 1991), Cabo de Gata (Franseen et al., 1998), and Sorbas (Martín et al., 1993; Boruillot et al., 2010).

Concerning the depositional interpretation, synthem MII records a gradual evolution of three environments, which, from the most proximal to the most distal, are: (1) a carbonate beach corresponding to system MIIb(o), which represents the foreshore, with swash-backwash processes, and the upper shoreface, with oscillatory flows and coastal currents; (2) a lower shoreface and inner shelf (MIIb), dominated by storm ebb surges (sandstone beds); and (3) an outer shelf–basin (MIIa), where marly sedimentation, including frequent low-energy distal

tempestites, alternates with the precipitation of selenite gypsum.

Consequently, as a whole, synthem MII is interpreted as a shallowing-upward sequence. Thus, as expressed in Figure 3A, the MIIb(o) system (carbonate beach) interfingers with MIIb (sandstone beds interbedded with sandy marls, inner shelf), and the latter interfingers with MIIa (gypsum beds interbedded with marls). Note that the stratigraphic organization scheme represented in Figure 2A considers MIIb and MIIb(o) as a shallow-marine shelf and beach for the sake of synthesis.

The strontium and sulfur isotopes indicate that gypsum precipitated from marine brines with fluctuating salinities (Playà et al., 2000). Interbedded marls and gypsum are typical of Messinian basins in the Mediterranean area (see the Sorbas, Sicily, and Apennines basins; e.g. Martín and Braga, 1994; Riding et al., 1998; Krijgsman et al., 2001; Roveri et al., 2001, 2008; Braga et al., 2006) and might define astronomical precessional cycles (Krijgsman et al., 2001; Roveri et al., 2014). In San Miguel de Salinas, the first record of branching selenite occurs in gypsum bed G6. Although inconclusive, the common appearance of branching selenite facies from the 6th cycle upwards might be a particularly good marker bed for the correlation of the various evaporitic basins throughout the Mediterranean (Roveri et al., 2014).

The upper MIIb depositional system is truncated by an erosional surface corresponding to the end-Messinian unconformity. Overlying this unconformity, synthem P marks the start of Pliocene sedimentation.

4.2.3. Synthem P

The most complete succession of synthem P can be seen in the Canal section (Fig. 3B), where the three marine depositional systems (P0, P1, and P2) are well exposed. As illustrated in Figure 3A, the Canal section coincides with a 40 meter-deep paleovalley, termed the San Miguel paleovalley, which laterally continues as a flat erosional surface represented in the

Km16 and Lo Rufete sections. This flat, intensely bioturbated surface is modeled over the MIIb sandstones and the oolitic grainstones (MIIb(o)), and is covered by the P2 sandstones (Fig. 8 A and B). Both morphological features characterized the end-Messinian unconformity in the San Miguel de Salinas sector.

The P0 depositional system comprises two conformably stacked lithological assemblages. A 2-m thick conglomerate bed made up of heterometric clasts derived from the underlying sandstone layers (synthem MII) represents the lower assemblage. Its scant lateral continuity indicates that this body fills the bottom of the San Miguel paleovalley. The clasts are matrix-supported, up to 10 cm in diameter and have high textural maturity, characterized by well-rounded, subspherical, and discoid morphologies (Fig. 8C). The upper assemblage is made up of 4-m thick, coarse-grained yellowish sandstones rich in ostreids, pectinids, and echinoids.

The P1 depositional system conformably overlies the P0 system and is represented by a 30-m thick yellow marl succession rich in foraminifera and calcareous nannoplankton. It contains thin beds (structureless or with diffuse planar lamination) of fine-grained terrigenous sandstones (Fig. 8D) characterized by abundant *Thalassinoides* (Fig. 8F) and common broken pectinid shells.

The P1 system gradually changes upwards to the P2 system, with the sandstone beds increasing in number and thickness and the marly interbeds decreasing in number and thickness. Both lithologies are cyclically arranged (Fig. 8G and E). The terrigenous sandstones of the P2 system show HCS of gentle-undulated laminae. To the top of the P2 system, the marly interbeds disappear. On the whole, the P1 and P2 depositional systems form a thickening-upward succession of sandstone beds, in accordance with the progradational pattern illustrated in Figure 3A.

Overall, synthem P represents the re-establishment of open marine conditions in the San Miguel de Salinas sector after the end-Messinian unconformity. The basal P0 conglomerate is

interpreted as a coastal lag (gravel beach) immediately followed by sediments rich in shallow-water marine shells. This basal lag (transgressive systems tract) at the bottom of synthem P was ubiquitously observed in the Bajo Segura basin and is particularly well exposed in its northern margin (Caracuel et al., 2004, 2011). These deposits represent the transgression after the lowstand-related erosion that gave rise to the San Miguel paleovalley. The erosional surface at the bottom of synthem P is interpreted as a polygenic surface that resulted from the combined effect of the lowstand erosion plus the transgressive wave ravinement of the marine environment after the sea-level rise. This erosional phase has been documented in several places in the Bajo Segura basin and has been related to a major sea-level drop (lowstand sea-level phase, after Caracuel et al., 2004; Corbí, 2010; Soria et al., 2005, 2008a, 2008b; Martínez del Olmo, 2011). System P1 corresponds to the establishment, due to sea-level rise, of open marine environments favorable to the development of nannoplankton and foraminifera. System P2 records the development of a storm-dominated, shallow-water platform with a continental sediment supply. The progradation of this platform over the marly deposits of the basin generates the shallowing-upward, regressive sequence of the P1-P2 succession, which characterized the highstand. In short, the evolution from the P0 to P1 systems records the platform transgression, and the evolution from the P1 to P2 systems records the platform progradation.

5. Chronostratigraphy

5.1. Biostratigraphy

For the planktonic foraminifer biozonation, we adopted the Mediterranean zonal scheme proposed by Iaccarino et al. (2007), in which the ages and magnetochronological calibrations of biozones are based on Lourens et al. (2004). For nannoplankton, we have considered the biozonation of Okada and Burky (1980), their data having been astrobiochronologically calibrated by Raffi et al. (2006) Only the most significant bioevents (Fig. 3B) for each synthem

are listed in the following paragraphs.

5.1.1. Synthem Messinian I

The most important bioevents recorded in this synthem are:

(1) The occurrence of the *Globorotalia miotumida* group dominated by the *Globorotalia mediterranea* species. In the Mediterranean, the first common occurrence (FCO) of the *Globorotalia miotumida* group defines the Tortonian/Messinian boundary (Sierro et al., 1985 1993; Hilgen et al., 2000a, 2000b).

(2) The dominance of dextrally coiled *Neogloboquarina acostaensis*. The change from sinistral to dextral coiling of *N. acostaensis* is dated at 6.35 Ma, chron C3An1r (Lourens et al., 2004).

(3) The occurrence of *Bulimina echinata*. The FO of this species is dated at 6.29 Ma (Kouwenhoven and Van der Zwaan, 2006).

(4) The presence of *Amaurolithus delicatus*. The Tortonian/Messinian boundary coincides almost exactly with the first regular occurrence of the *Globlorotalia miotumida* (*conomiozea*) group (Sierro, 1985) and the FO of *A. delicatus*, although the latter slightly postdates the boundary (Hilgen et al., 2000a, 2000b; Lourens et al., 2004).

(5) The continuous record of *Reticulofenestra rotaria*. The FCO of *Reticulofenestra rotaria* coincides with the FO of *Amaurolithus delicatus* and is considered the second event that marks the beginning of the Messinian (Hilgen et al., 2000a, 2000b; Rafi et al., 2003; Morigi et al., 2007). The last common occurrence (LCO) has been established at 6.79 Ma (Lourens et al., 2004; Negri et al., 1999). The last specimens of *Reticulofenestra rotaria* reach the top of chron C3An.1n (Lancis et al., 1998; Hilgen and Krijgsman, 1999; Krijgsman et al., 1999).

(6) The presence of *Reticulofenestra pseudoumbilicus* >7 µm at percentages greater than 2% of the nannoflora assemblage. These percentages indicate a location above the top of the

paracme (PE) of *Reticulofenestra pseudoumbilicus*, established in the Mediterranean at 7.167 Ma (Hilgen et al., 1995, 2000a, 2000b; Raffi et al., 2003, 2006).

(7) The presence of *Nicklithus amplificus,* with a FO calibrated at 6.68 Ma, at the base of chron C3An.2n (Lancis, 1998; Raffi et al., 2003). The last specimen of *Nicklithus amplificus* is recorded at the top of chron C3An.1n. This level marks the beginning of the Messinian Salinity Crisis in the Mediterranean (Krijgsman et al., 1999; Raffi et al., 2003).

5.1.2. Synthem Messinian II

This synthem is characterized by the following events:

(1) The presence of *Globorotalia mediterranea* and dextrally coiled *Neogloboquadrina acostaensis.*

(2) The record of dwarf fauna of planktonic foraminifera, mainly represented by *Globoturborotalita apertura*/*Globoturborotalita decoraperta*, *Globigerina bulloides,* and *Neogloboquadrina* spp. In the Mediterranean, dwarf fauna of planktonic foraminifera have been documented in several sections and DSDP sites (e.g. Sorbas basin: Riding et al., 1998; Martín et al., 1999; Braga et al., 2006; Almería-Níjar basin; Aguirre and Sánchez-Almazo, 2004; sites 974, 975 and 978: Iaccarino and Bossio, 1999; site 42A: Cita et al., 1978).

(3) The presence of *Amaurolithus delicatus and Reticulofenestra pseudoumbilicus* >7 μm.

(4) The absence of *Reticulofenestra rotaria* and *Nicklithus amplificus.*

5.1.3. Synthem Pliocene

The main events for the Pliocene are:

(1) The abundance of *Globigerinoides* spp. (*G. trilobus*, *G. obliquus*, *G. extremus*), typical of the base of the Pliocene in the Mediterranean (Iaccarino et al., 1999).

(2) The occurrence of *Ceratolithus acutus*, which appears (FO) at 5.32 (Lourens et al., 2004). In the Mediterranean, the First Appearance Datum (FAD) of *C. acutus* was delayed until the beginning of the Pliocene (Cita and Gartner, 1973; Castradori, 1998) because of the isolation of the basin during the Messinian Salinity Crisis.

(3) The occurrence of *Reticulofenestra cisnerosii*. The FO of *R. cisnerosii* has been proposed as an alternative or complementary event to define the base of the Pliocene in the Mediterranean (chron C3r, Lancis and Flores, 2006). This has also been observed by Di Stefano and Sturiale (2010), who record the presence of "*Reticulofenestra zancleana*" (a junior synonym of *Reticulofenestra cisnerosii*; Lancis and Flores, 2006) at the base of the Pliocene in chron C3r in several sections of the Mediterranean and in ODP Leg 160 in the Mediterranean.

(4) The abundance and diversity of asteroliths, which characterizes the bottom of the Pliocene (Lancis, 1998).

(5) The occurrence of *Ceratolithus rugosus* in the upper part of the SMdS (Fig. 3B). The FO of *Ceratolithus rugosus* marks the base of the CN10c subzone (Okada and Bukry, 1980) and the NN13 zone (Martini, 1971) occurring in the equatorial Atlantic during chron C3n.4n (Thvera) at 5.05 Ma, and in the equatorial Pacific at 5.12 Ma (Backman and Raffi, 1997; Lourens et al., 2004; Raffi et al., 2006). The scarcity of *Ceratholitus rugosus* does not allow a confirmation of the FO in the sampling.

5.2. Magnetostratigraphy

The intensity of the NRM is relatively weak in the studied rocks, ranging between 0.05 mA/m and 0.15 mA/m. Upon stepwise demagnetization, two components can normally be distinguished in addition to a small viscous component removed at the first demagnetization step, likely related to handling and/or storage. A low-field component corresponding to the present geomagnetic field is removed up to fields of 17–21 mT. Then, a characteristic

remanent magnetization (ChRM) is removed up to the maximum field applied (100 mT), which trends towards the origin of the diagram and has dual polarity (Fig. 4). We have established a ranking based on the quality of the demagnetization trajectories. Class A includes samples for which the ChRM component can be calculated unambiguously. Class B denotes samples with ambiguous ChRM components, and class C non-interpretable demagnetization trajectories.

The VGP latitudes derived from the class A ChRM yield a succession of two magnetozones in the Lo Rufete, Km16, and lower part of the Canal sections characterized by reverse polarity. In this latter section, normal polarity has been interpreted for the uppermost samples (Fig. 3B). The lower part of the Lo Rufete section includes four unreliable class B samples and only one reverse class A sample (upper one). Therefore, this interval is reported as ambiguous in polarity and depicted in gray on the polarity column in Figure 3B. The upper part of the Canal section shows an interval of class B samples, also shown in gray.

5.3. Chronostratigraphic framework

The integration of the biostratigraphic and magnetostratigraphic data in the SMdS section has served to establish the time interval recorded in the three synthems (Fig. 3B).

In synthem MI, the presence of *Globorotalia miotumida*, *Amaurolithus delicatus,* and *Reticulofenestra pseudoumbilicus* >7 µm points to a Messinian age. The record of *Reticulofenestra rotaria, Nicklithus amplificus, Bulimina echinata,* and the predominance of dextral-coiled *Neogloboquadrina acostaensis* restricts the time interval to the upper Messinian (between chron C3An1r and the base of C3r). This calibration is consistent with the biomagnetostratigraphic calibration proposed by Soria et al. (2008a, 2008b) for the upper part of synthem MI recorded in the nearby Garruchal and La Pedrera sections.

Synthem MII could be assigned to the upper Messinian, specifically to chron C3r, on the basis of the reverse polarity and presence of *Globorotalia mediterranea*, dextral-coiled

Neogloboquadrina acostaensis, Amaurolithus delicatus, and Reticulofenestra pseudoumbilicus >7 µm*,* the absence of *Reticulofenestra rotaria and Nicklithus amplificus,* and the dominance of dwarf fauna of planktonic foraminifera.

The presence of *Ceratolithus acutus* and *Retiulofenestra cisnerosii* (Lancis and Flores, 2006) assigns the bottom of synthem P to the lowest Pliocene (Fig. 3B). This is also consistent with the record of the acme of *Sphaeroidinellopsis* spp., observed at the base of this synthem in adjacent sections (e.g. La Pedrera section in Corbí, 2010 and referred to the base of the Pliocene; biozone MPl1). This event was not recorded in the study section, most probably because these taxa are restricted to pelagic environments (Iaccarino et al., 2007). The occurrence, although scarce, of *Ceratolithus rugosus* in the upper part of the Canal section (Fig. 3B) does not allow the FO to be established in the sampling. Therefore, the magnetobiostratigraphic data do not allow the chrons in the Pliocene synthem of the Canal section to be accurately assigned. Consequently, the upper inverse samples of this section could be assigned to chron C3n.3r or C3n.2r, and the top normal interval of the section to chron C3n.3n or C3n.2n respectively (Fig. 3B).

6. Foraminifer and nannoplankton analysis and paleoenvironmental interpretation

The foraminifer and nannoplankton data are shown in figures 9, 10, and 11. The most significant paleoenvironmental features for each synthem are listed in the paragraphs below.

6.1. Synthem Messinian I

In the depositional system MIa, planktonic foraminifera are abundant, representing more than 75% of the total foraminifer content in some samples. Assemblages are highly diverse and dominated by *Globigerina bulloides*, *Globoturborotalita apertura/decoraperta*, *Neogloboquadrina continuosa*, *Neogloboquadrina acostaensis,* and *Neogloboquadrina* sp. Fluctuations were recorded in the warm-oligotrophic/cold-eutrophic ratio related to

planktonic foraminifer distribution (samples 1 to 7 in the Lo Rufete section).

In the MIa, the benthic diversity of foraminifer assemblages is high. Taxa typical of shelf environments such as *Ammonia beccarii*, *Elphidium crispum*, *Elphidium macellum*, *Cibicides dutemplei*, *Cibidides lobatula,* and *Textularia* sp. dominate, although occasional deep-water taxa (*Melonis pompillioides*, *Pullenia bulloides,* and *Uvigerina* sp.) were observed. The sporadic presence of *Valvulineria bradyana, Bulimina* spp. (mainly *Bulimina aculeata* and *Bulimina echinata),* and *Elphidium granosum* was recorded. *Valvulineria bradyana* is considered as an indicator of sediment enriched in organic matter where environmental stress conditions, such as hypoxia, occur periodically (Jorissen, 1988; Fontanier et al., 2002). *Bulimina aculeata* is a typical species in extremely eutrophic and dysoxic settings (Fontanier et al., 2002). *Bulimina echinata* is a species adapted to low-oxygen contents and abundant organic matter (Kouwenhoven and Van der Zwaan, 2006). *Elphidium granosum* is typical of restricted environments (Debenay et al., 2000).

A marked decrease in diversity of foraminifera and nannoplankton was observed in the transition from MIa to MIb. In the latter, planktonic foraminifera are almost absent and benthic foraminifer assemblages are dominated by *Ammonia beccarii*, typical of inner shelf environments.

In the nannoplanktons, asteroliths are scarce throughout synthem MI, slightly decreasing from the bottom towards the top of the synthem. Small placoliths are abundant in the entire synthem, whereas *Reticulofenestra pseudoumbilicus* (5–7 µm) is common. The upper part of the synthem is characterized by a smaller amount of *Reticulofenestra pseudoumbilucus* (>7 µm) and asteroliths compared to the lower part.

The foraminifer assemblages confirm a shelf environment grading distally to a marine basin, as also indicated by the coexistence of reticulofenestrids, asteroliths, and small placoliths.

The presence of stress markers such as *Bulimina aculeata*, *Valvulineria bradyana,* and *Bulimina echinata* suggests a slight bottom stress related to low oxygen conditions. This typical benthic assemblage, together with the abnormal abundance of planktonic foraminifera (in several samples up to 50%, a percentage typical of bathyal environments, Van der Zwaan et al., 1990), is most probably due to water column stratification.

The alternation of gray and light tobacco-colored marls, together with changes in the cold-eutrophic/warm-oligotrophic planktonic ratio, is a characteristic feature of the lower part of the synthem. Equivalent facies alternation is recorded in the Sorbas basin where, according to Krijgsman et al. (2001), it is predominantly related to precession-controlled dry–wet oscillations in a circum-Mediterranean climate. These climate oscillations can cause changes in water temperature and trophism, which are recorded in the evolution of planktonic foraminifer assemblages (Sierro et al., 2003; Sánchez-Almazo et al., 2007).

A shallowing-upward trend from the bottom to the top of the synthem is evidenced by the evolution of the sedimentary features and the nannoplankton and benthic foraminifer assemblages. This change is marked by a decrease in diversity of foraminifera and nannoplankton and by the dominance of benthic foraminifera, exclusively represented by *Ammonia beccarii*. Note that the %P evolution does not show this shallowing trend in the MIa system (Fig. 9), with high percentages remaining during the system evolution. We interpret this unique feature to be a consequence of water column stratification, where abnormal abundances of planktonic foraminifera in the samples can be related to low oxygen conditions in the bottom, which leads to low diversity and abundance in the benthic foraminifer assemblages. In contrast, system MIb has %P ratios close to 0%, which confirms the shallowing-upward trend of synthem MII.

6.2. Synthem Messinian II

As explained in the stratigraphy and sedimentology section, the most typical feature of this

synthem is the interbedded gypsum and marly layers that represent the record of repetitive environmental changes in the water column. Foraminifera and nannoplankton are used as proxies to characterize the environmental conditions present during the inter-evaporitic phase.

Foraminifera are less abundant than in synthem MI. The planktonic/benthic foraminifer ratio is highly variable, ranging from planktonic-dominated assemblages to benthic-dominated ones.

Dwarf forms of planktonic foraminifera (*Globoturborotalita apertura*/*Globoturborotalita decoraperta*, *Globigerina bulloides,* and *Neogloboquadrina* spp.) were recorded. We consider these fauna to be autochthonous since no reworking is recognized, as generally evidenced by the good preservation of the tests and the absence of abrasion, dissolution, and fragmentation. Consequently, our taphonomic observations and the paleoenvironmental analysis indicate these dwarf fauna are likely the record of stressed marine conditions in the water column, as pointed out by Bolwovskoy and Wright (1976) for the dwarfism in benthic foraminifera. This interpretation is in consonance with proposals for equivalent deposits in the Sorbas basin by Riding et al. (1998) and Braga et al. (2006) and in the Almería-Níjar basin by Aguirre and Sánchez-Almazo (2004).

Benthic foraminifera are mainly represented by *Ammonia tepida*, *Elphidium granosum,* and *Elphidium williamsoni*. The occasional presence in some samples of *Ammonia beccarii*, *Bulimina costata*, *Cibicides* spp., *Elphidium crispum*, *Elphidium advenum*, *Elphidium macellum, Nonion commune*, *Reusella spinulosa*, *Textularia* sp., and *Valvulineria bradyana* is observed. *Ammonia tepida*, *Elphidium granosum,* and *Elphidium williamsoni* are related to restricted environments such as lagoons, estuaries, or restricted bays (Debenay et al., 2000). In particular, *Ammonia tepida* are normally interpreted as representative of brackish waters (e.g. Cita et al., 1978; Iaccarino and Bossio, 1999). However, broadly speaking, these species are euryhaline and have also been recorded in high-salinity environments (Zainnetti, 1982, 1984;

Murray, 2006). According to Van der Zwaan (1982), the distribution pattern of *Reusella spinulosa* suggests a slight tolerance to increased salinities and oxygen deficiency.

Asteroliths and small placoliths are less abundant than in synthem MI; dwarf asteroliths and dwarf placoliths (mainly *Coccolithus pelagicus* spp., *Calcidiscus* spp., *Geminitella* spp., and *Helicosphera* spp.) were recorded throughout the entire synthem. Noteworthily, dwarf and normal-sized forms of asteroliths (*Calcidiscus* spp., *Umbilicosphaera* spp., *Coccolithus pelagicus,* and *Amaurolithus* spp.) are sometimes found coetaneously. The contemporary *Reticulofenestra pseudoumbilicus* (7 µm and 5–7 µm) is generally very rare, but a marked increase in abundance was recorded in a few samples (samples 5 in the Km16 section and sample 17 in the Canal section).

Overall, the marly intervals of synthem MII are indicative of a restricted marine basin with bottom-water stagnation and stratification together with episodic evaporitic precipitation. The benthic assemblage dominated by *Ammonia tepida*, *Elphidium granosum,* and *Elphidium williamsoni* indicates marked stress on the bottom caused by low oxygen and hypo- or hyperhaline conditions. Stressful conditions in the water column are revealed by the abundance of dwarf forms of planktonic foraminifera (Boltovskoy and Wright, 2013) such as *Globoturborotalita apertura*/*Globoturborotalita decoraperta, Globigerina* spp., *Neogloboquadrina* spp. This is consistent with the decrease in nannoplankton abundance and the presence of dwarf asteroliths and dwarf placoliths (Müller, 1978, 1990; Lancis, 1998). The coexistence of dwarf and normal-sized forms of nannoplankton and the occasional increase in *Reticulofenestra pseudoumbilicus* (7 µm and 5–7 µm) abundance points to scattered intervals of normal marine water (Müller, 1990).

Major changes in water salinity and bottom-water oxygenation are recorded by the alternation of gypsum precipitation and laminated marl sedimentation together with the fluctuations in foraminifer and nannoplankton assemblages. The development of selenite gypsum provides

important paleoenvironmental information since it precipitates in oxic environments once the average salinity has reached the saturation value for gypsum (145 g/l) (Sloss, 1969; Krijgsman and Meijer, 2008; Roveri et al., 2014). In contrast, the marly intervals record major changes in salinity in low oxygenation conditions, causing the particular foraminifer assemblage found in these deposits and evidencing stressed environmental conditions. The alternation of gypsum/marls may be caused, although inconclusively, by precession-controlled dry-wet oscillations such as Krijgsman et al. (2001) proposed for the gypsum/marl cycles in the Sorbas Basin. Gypsum formed during insolation minima (precession maxima) intervals, during dry periods and water mixing, when evaporation was greater than freshwater input. In contrast, laminated marl deposition indicates periods of insolation maxima (precession minima), a relatively wet climate, stratified waters, and low bottom oxygenation.

6.3. Synthem Pliocene

Fifty-two species of benthic foraminifera and 31 species of planktonic foraminifera were recorded, with a clear increase in both abundance and diversity with respect to the MII assemblage. The planktonic foraminifer assemblage is dominated by *Globigerinoides* spp. (mainly *Globigerinoides trilobus* and *Globigerinoides obliquus*).

Benthic foraminifera typical of littoral, inner shelf environments (%P < 15) dominate at the base of synthem P1. The most significant taxa are *Ammonia beccarii*, *Amphistegina lessonii*, *Biasterigerina planorbis*, *Cibicides dutemplei*, *Cibicides lobatula,* and *Elphidium crispum*, which represent an assemblage characteristic of sandy bottoms. Diversity and %P reach their highest values in system P1 (sample 20), where foraminifera typical of shelf environments dominate (*Ammonia* spp., *Cibicides dutemplei*, *Cibicides lobatula*, *Elphidium* spp., *Nonion commune*, *Reusella spinulosa,* and *Textularia gramen*), although forms related to deeper environments (*Pullenia bulloides* and *Uvigerina bononiensis*) are occasionally present. A decrease in diversity and in the abundance of planktonic foraminifera is recorded from P1 to P2. The most

significant benthic taxa of the P2 system are *Ammonia beccarii*, *Cibicides* spp., *Elphidium* spp., and *N. commune*, all of them typical of inner shelves. The environmental stress markers *Bulimina aculeata*, *Bolivina* spp., and *Valvulineria bradyana* were occasionally recorded throughout the entire synthem P, together with *Elphidium granosum*, typical of restricted environments.

The nannoplankton record is continuous and without significant fluctuations throughout the entire synthem, but representing an evident change with respect to synthem MII. Notably, dwarf asteroliths and dwarf placoliths are absent in synthem P, whereas normal-sized asteroliths are more diverse and abundant. *Reticulofenestra pseudoumbilicus* (>7 µm and 5–7 µm) are present throughout the whole synthem; small placoliths are abundant.

Variations in %P and benthic foraminifer assemblages point to subsequent deepening and shallowing trends, with the maximum depth reached in system P1. The occasional presence of paleoenvironmental stress (*Bulimina aculeata*, *Bolivina* spp., and *Valvulineria bradyana*) and restricted environment markers (*Elphidium granosum*) points to a slight bottom stress, most probably related to episodes of low oxygenation. The abundance of small placoliths is related to periods of high nutrient content due to continental runoff and/or river input (Aubry, 1992; Lancis, 1998; Wade and Bown, 2006).

As also proposed by Caracuel et al. (2011) and Corbí (2010), in the first step of the Pliocene transgression, paleovalleys incised in the Messinian are filled by shallow-marine and coastal deposits. The following phase ended with a highstand and the new coast and platform systems prograded onto the previously deposited open marine sediments. The occasional presence of benthic foraminifer stress markers would be related to periodic low bottom oxygenation. These low oxygen levels could have been induced by limited bottom circulation because of the presence of bays and flooded paleovalleys representing relatively restricted environments.

7. Discussion: Insights into the puzzle of the Messinian Salinity Crisis

The synthetic depositional model proposed in this work includes the following phases: (1) late-Messinian pre-evaporitic marine deposits (synthem MI) that record a shallowing-upward trend with changes in trophism and water temperature; (2) emersion and erosion (intra-Messinian unconformity) at the top of synthem MI predating the gypsum deposition; (3) marine reflooding leading to the deposition of synthem MII during chron C3r; (4) a gradual vertical change from gypsum deposits alternating with marls and sandstones, where foraminifer and nannoplankton assemblages record a stressed marine environment (MIIa system) to a sandstone-dominated interval (MIIb) and carbonate-dominated oolitic grainstones (MIIb(o) system); (5) end-Messinian erosional surface represented by an incised paleovalley; and (6) marine Pliocene deposition recording the reflooding of the previously incised paleovalleys.

To evaluate the regional significance of the stratigraphic model of the San Miguel de Salinas sector, we assess the possible correlation with other Neogene basins of SE Spain documented by different authors. First, an intra-Messinian unconformity underneath the gypsum unit detected in the San Miguel de Salinas area is in disagreement with the two-step model of the Messinian Salinity Crisis suggested by Clauzon et al. (1996). Clauzon´s model proposes a gradual transition from the pre-evaporitic marine deposits to the Yesares evaporites for the Sorbas and Almeria-Níjar basins. Such a gradual evolution from pre- to syn- evaporitic deposits, specifically proposed by several authors for the Sorbas basin (Krijgsman et al., 2001; Sierro et al., 2001, 2003), has not been detected in the San Miguel de Salinas area, in which the intra-Messinian unconformity is clearly below synthem MII, hence separating the pre- from the syn-evaporitic unit. In addition, our depositional model seems to diverge from the recent synthetic model proposed by Clauzon et al. (2015) for the Sorbas basin, in which they cite an unconformity separating the gypsum/marl alternations from the overlying sandstones and oolitic grainstones. In contrast, in the San Miguel de Salinas composite section, a gradual facies evolution is recorded from gypsum/marl deposits (MIIa) to siliciclastics (MIIb) and oolitic grainstones (MIIb(o)).

On the other hand, the stratigraphic model, based on the Almería basins, proposed by Martín and Braga (1994), Riding et al. (1998, 1999), Aguirre and Sánchez-Almazo (2004), and Braga et al. (2006) seems to be generally applicable to the San Miguel de Salinas sector. According to our stratigraphic model, synthem MIIa (syn-evaporitic unit) is equivalent to the evaporites of the Yesares Member of the Sorbas and Almería basins, and the overlying MIIb system seems to be equivalent to the post-evaporitic Sorbas deposits (alternating marls and coarse terrigenous sediments) of the Sorbas basin and the Feos Formation (siliciclastic deposits) of the Almería-Níjar basin. Finally, the oolitic grainstones of the MIIb(o) system are equivalent to the Terminal Complex Carbonates. Furthermore, as stated above, our depositional model reveals an intra-Messinian unconformity (erosional surface) underneath the syn-evaporitic unit (synthem MII), followed by Messinian marine reflooding, which has also been reported by Braga et al. (2006) in the neighboring Sorbas and Almería-Níjar basins. Although the stratigraphic model of Braga et al. (2006) is largely applicable to the San Miguel de Salinas sector, as mentioned above, it differs slightly in the interpretation of the end-Messinian discontinuity, which separates the Messinian from the Pliocene. While Braga et al. (2006) consider that this unconformity is related mainly to uplift and tectonic re-structuring of the region, our data indicates that this major discontinuity represents deep incised paleovalleys, as reported by Soria et al. (2008a, 2008b) and Caracuel et al. (2011) in other sectors of the basin, which have been filled with Pliocene marine sedimentation. Consequently, the end-Messinian unconformity would be related, at least in the Bajo Segura basin, to a significant sea-level fall preceding the Pliocene marine reflooding of the basin, in agreement, on this point, with the model of Clauzon et al. (1996).

The stratigraphic scheme and the sedimentary and paleoenvironmental model derived from the present study (Fig. 12) reveal the key points noted below that can help to understand the Messinian Salinity Crisis recorded in the peri-Mediterranean marginal basins in southeastern Spain.

a) The intra-Messinian unconformity limits the pre-evaporitic unit and the evaporitic unit

This unconformity is recorded throughout the entire Bajo Segura basin (Soria et al., 2008b, 2014, and references therein). As explained above (and considering a regional-scale correlation), the intra-Messinian unconformity is in the same stratigraphic position as the "sub-Yesares erosional surface" described by Riding et al. (1998, 1999, 2000), Aguirre and Sánchez-Almazo (2004), and Braga et al. (2006) for the Sorbas and Níjar basins. According to these authors, this surface separates the Abad marls from the overlying Yesares gypsum. In the marginal areas of the Níjar Basin, according to Lu (2006), Yesares gypsum clearly overlies different Abad marl beds in an unconformable contact with a paleokarst. In other Betic basins, such as the Fortuna Basin, Garcés et al. (1998) pointed out that the change from the alluvial-palustrine member to the prograding conglomerate member records a sea-level fall associated with the beginning of the Messinian Salinity Crisis. This change occurs in the lower part of chron C3r and, according to Soria et al. (2005), it can be correlated with the intra-Messinian unconformity in the Bajo Segura basin. Concerning the Sorbas basin, despite the abundant field data presented by Riding et al. (1999, 2000) on an erosional surface between the pre-evaporitic and the evaporitic units, other authors report that these two units are conformable, without any kind of hiatus between them (Fortuin et al., 2000; Sierro et al., 2001, 2003; Krijgsman et al., 2001; Manzi et al., 2013). According to these authors, the main arguments supporting this hypothesis are related to the complete record of the precessional cycles, that is, the absence of a gap between the two units and the presence of local unconformities related to gravitational sliding between the pre- and syn-evaporitic deposits. In contrast, the data gathered from the study of the San Miguel de Salinas sector evidence an unconformity, at least in the Bajo Segura basin, at the top of the pre-evaporitic unit. According to the stratigraphic model here proposed, the pre-evaporitic unit (synthem MI) forms a highstand regressive megasequence whose evolution was interrupted by a significant sea-level fall (intra-

Messinian unconformity). Consequently, the beginning of a new regressive sequence (evaporitic unit or synthem MII) is the result of renewed, complete flooding of the basin.

b) The intra-Messinian unconformity in exploratory wells

Ochoa et al. (2015) studied exploratory wells drilled close to the San Miguel de Salinas area (235-San Miguel de Salinas and 260-La Mata) and concluded that the offshore transition between the Tortonian-Messinian marls (pre-evaporitic unit) and the Primary Lower Gypsum (Evaporitic Unit) corresponds to an abrupt but non-erosional contact. Consequently, the same authors concluded that, in the distal parts of the basin, the transition to evaporitic beds occurred at 5.97 Ma. This hypothesis implies that the intra-Messinian erosional surface detected in San Miguel de Salinas would represent a limited sea-level fall recorded only in local marginal areas. Nevertheless, the erosional surface (intra-Messinian unconformity) detected below the syn-evaporitic unit has been considered as a major erosional surface recognized in the peri-Mediterranean basins as shown, for example, by Braga et al. (2006) and Riding et al. (1998, 1999) in the Sorbas Basin. In the Bajo Segura basin, this intra-Messinian unconformity can also be viewed as a major erosional surface, as can be inferred in this work, and in other sectors of the Bajo Segura basin (Soria et al., 2008a, 2008b). This apparent contradiction could be explained taking into account that "proximal erosional unconformities" (in our study area, the intra-Messinian unconformity detected in the Lo Rufete section) would pass laterally, in deep marine settings (exploratory wells, Ochoa et al., 2015), into their distally "correlative conformities" (sensu Vail et al., 1977). As a consequence, the abrupt change but apparently non-erosional contact detected in seismic lines could be interpreted as a discontinuity without an erosional hiatus (paraconformity) or a discontinuity in terms of a significant environmental change and, hence, equivalent to the intra-Messinian unconformity recorded in the San Miguel de Salinas area.

c) Dwarf fauna of planktonic foraminifera recording anomalous marine water conditions in the syn-evaporitic unit

One of the key paleoenvironmental issues in the San Miguel de Salinas composite section is the record of dwarf fauna of planktonic foraminifera in the interbedded marls associated with gypsum beds (syn-evaporitic unit). This particular foraminifer assemblage has also been documented in late-Messinian Mediterranean onshore sections and ODP sites (e.g. Cita et al., 1978; Hsü et al., 1978; Van de Poel, 1992; Iaccarino and Bossio, 1999; Fortuin and Krijgsman, 2003; Braga et al., 2006). The ecological significance of this unusual fauna is actually a significant point of discussion subject to opposing interpretations. In fact, several authors have considered this fauna (although inconclusively) as reworked (e.g. Iaccarino et al., 1999; Fortuin and Krijgsman et al., 2003; Bassetti et al., 2006). Other authors propose that they represent the late-Messinian marine record of Mediterranean reflooding (e.g. Riding et al., 1998; Aguirre and Sanchez-Almazo, 2004; Braga et al., 2006). The results of the present work, based on taphonomic observations and paleoenvironmental analysis, support the hypothesis that dwarf planktonic fauna (dominated by globoturborotalids, globigerinids, and neogloboquadrinids) record anomalous marine water conditions in the water column. Furthermore, the finding of dwarf asteroliths and dwarf placoliths reported in this work is congruent with this interpretation. Consequently, we suggest that the fluctuations in the abundance of dwarf planktonic foraminifera and euryhaline and stenohaline species of benthic foraminifera detected in the syn-evaporitic unit could be related to salinity changes in a stressed marine basin with bottom-water stratification and episodic evaporitic precipitation. Interestingly, the paleoenvironmental interpretation of this particular dwarf fauna as autochthonous marine planktonic foraminifera is in line with that proposed by Riding et al. (1998) for the Sorbas basin, and Aguirre and Sanchez-Almazo (2004) and Braga et al. (2006) for the Almería-Níjar basin, who all consider that small planktonic foraminifera are the record of the late-Messinian marine reflooding.

d) A different number of gypsum beds recorded in the San Miguel de Salinas area

The syn-evaporitic unit (synthem MII) of the San Miguel de Salinas area records a different number of gypsum beds depending on the stratigraphic section analyzed. For instance, the Lo Rufete section has no gypsum beds, the Km16 section records four, and the Canal section registers seven. Based on the stratigraphic relations proposed in this work, from proximal to distal, the number of gypsum beds increases in a progradational pattern. The lower number of gypsum beds in SMdS in comparison with neighboring Sorbas basin (15 gypsum cycles, Lugli et al., 2010) can be explained by the fact that selenite gypsum beds were deposited in the deepest part of the marginal Bajo Segura basin. According to this hypothesis, the more distal parts of the basin (not exposed in the southern Bajo Segura basin) record more gypsum beds than the proximal San Miguel de Salinas area. In fact, based on data from the exploratory wells, Soria et al. (2008a) and Ochoa et al. (2015) have detected nine gypsum beds in the 235-San Miguel de Salinas 1 well and 12 gypsum beds (Ochoa et al., 2015) or 15 (Soria et al., 2008a) in the 260-La Mata well. Consequently, the syn-evaporitic unit represented in the deepest part of the basin (in particular in the 235-San Miguel de Salinas well) could be registering a similar range of cycles (14–16 gypsum beds) as in the Mediterranean reference sections reported by Luigli et al. (2010), Roveri et al. (2014), and Krijgsman et al. (2001) for SE Spain and Vena del Gesso basin in NE Italy.

Another question is related with the dating of the onset of evaporite sedimentation in SE Spain. As pointed out by Braga et al. (2006) for the Sorbas and Níjar basins, but also applicable to the San Miguel de Salinas area, the erosional surface beneath the syn-evaporitic unit (intra-Messinian unconformity) would impede determination of the age for the beginning of gypsum formation in the marginal basins of SE Spain based on the dating of the top of the pre-evaporitic unit. Consequently, is difficult to show the synchronous onset of Messinian evaporite precipitation in the Mediterranean. Some data in the Bajo Segura basin point to the

local character of gypsum deposition, which probably does not follow a common, single pattern throughout the Mediterranean.

e) Absence of Lago-Mare facies over the evaporitic unit

In most of the basins in the Mediterranean domain, the evaporitic unit dominated by selenitic gypsum (Lower Primary Gypsum, according to CIESM, 2008) is overlain by the Lago-Mare-Upper Gypsum Unit. This unit marks the end of sedimentation in the Messinian. A diagnostic feature of the Lago-Mare unit is the presence of brackish to freshwater fauna and flora with Paratethyan affinities (Orszag-Sperber, 2006; Roveri et al., 2014). In the composite SMdS section, the Lago-Mare unit is absent and the oolitic grainstones at the top of the evaporitic unit (synthem MII), corresponding to the Terminal Carbonate Complex (Esteban, 1979), are truncated by the end-Messinian unconformity.

In the nearby Sorbas and Níjar basins, many authors have correlated the Sorbas-Zorreras Members and the Feos Formation with the brackish-freshwater deposits of the Lago-Mare (see recent update of the MSC by Roveri et al., 2014). Nevertheless, this equivalence to the Lago-Mare unit, in terms of paleoenvironmental interpretation, should be viewed with caution since both the Sorbas/Terminal Complex and the Feos deposits (post-evaporitic unit) contain unquestionably marine fossils, including coral patch reef (Martín et al., 1993; Braga et al., 1995, 2006), which is indicative of a clear marine influence (Aguirre and Sánchez-Almazo, 2004). Following this line of argument, the lack of the Lago-Mare unit in the San Miguel de Salinas area is indicative of these types of brackish-freshwater deposits never having formed there since synthem MII was deposited in marine settings. Naturally, an alternative approach could consider that the Lago-Mare unit in San Miguel de Salinas was completely eroded away at the end of the Messinian as a consequence of the sea-level fall that produced the end-Messinian unconformity. In this regard, it should be further noted that other marginal basins in the western Mediterranean do not record the Lago-Mare unit, as observed in the study area.

In the Melilla basin, for example, a basin-wide unconformity (late-Messinian erosional surface) separates the Terminal Carbonate Complex (or Cycle 2) from the open marine marls (or cycle 3, late Messinian?–Pliocene) (Munch et al., 2006). According to these authors, the Lago-Mare deposits are completely lacking, whether undeposited or eroded prior to the cycle 3 transgression.

Taking into account the northern sector of the Bajo Segura basin, late-Messinian lagoonal sedimentation represented in synthem MII, which contains *Cyprideis* and *Ammonia tepida*, have been associated to the Mediterranean Lago-Mare facies (Soria et al., 2007). This northern sector represents proximal basin settings (Soria et al., 2005, 2008a, 2008b) and, consequently, could be equivalent to the upper part of synthem MII (MIIb(o) carbonate-dominated oolitic grainstones (associated to the Terminal Carbonate Complex) represented in the San Miguel de Salinas area. Indeed, it could be argued that, in the Bajo Segura basin (pending confirmation), the sedimentation associated to the Lago-Mare unit (Soria et al., 2007) probably represents the proximal facies of the Terminal Carbonate Complex represented in the area. In any case, as proposed by Aguirre and Sánchez-Almazo (2004), we consider that the Lago-Mare deposits should be regarded as a particular type of facies with a questionable chronostratigraphic value representing brackish-freshwater deposits not necessarily formed synchronously all over the Mediterranean.

f) The end-Messinian unconformity represents a major stratigraphic boundary separating the evaporitic unit from the post-evaporitic one (synthem Pliocene)

The data from the SMdS section confirm that an unconformity developed at the Messinian/Pliocene boundary throughout the entire Bajo Segura basin (Soria et al., 2008a, 2008b; Caracuel et al., 2011, 2004; Corbí, 2010; García-García et al., 2011). In the study area, the end-Messinian unconformity corresponds to a truncation surface locally carved by the San Miguel paleovalley. Along the axis of this paleovalley, the upper part of the oolitic synthem MII

was completely eroded. Other larger paleovalleys located outside of the study area, such as Crevillente (Soria et al., 2005) and La Pedrera (Martínez del Olmo and Serrano Oñate, 2000; Soria et al., 2008a), allow the end-Messinian unconformity to be correlated with a sea-level fall prior to the Mediterranean Pliocene reflooding. We support a polygenic character for this unconformity, which derived from two different erosional processes. The first process is strong incisement by rivers and channels because of the sea-level fall. The second process is coastal ravinement during the sea-level rise associated with the Pliocene transgression. It is evident that this second process alone cannot explain the significant erosional features of the unconformity. We can consider the La Pedrera paleovalley as an example, where erosion deleted more than 200 m of sediments (i.e. the top of synthem MI and the entire synthem MII). In fact, according to Soria et al. (2008b), in the La Pedrera section, the basal conglomerates at the bottom of synthem P lie directly upon the marl-sapropel-diatomite cycles of synthem MI, representing a hiatus of about 0.6 Ma.

8. Conclusions

The good exposure of the outcrops and the ample distribution of planktonic and benthic foraminifer and nannoplankton assemblages in the pre-, syn-, and post-evaporitic deposits suggest that the SMdS composite section (Fig. 12) is one of the most suitable records to analyze the progression of the events related to the Messinian Salinity Crisis in the western Mediterranean margins.

Based on the sedimentological, biostratigrafic (foraminifera and nannoplankton), and magnetostratigraphic data, the following phases have been identified: synthem MI (pre-evaporitic), which developed during the late-Messinian, synthem MII (syn-evaporitic), which took place in chron C3r, and synthem P (post-evaporitic) in the early Pliocene.

All the data allow a characterization of the paleoenvironmental evolution of each phase. Synthem MI (pre-evaporitic phase) represents a shallowing-upward trend, where the

alternation of gray and light tobacco-colored marls together with variations in the cold-eutrophic/warm oligotrophic planktonic foraminifer ratio can represent cyclic changes in trophism and water temperature, probably related with precession-controlled dry-wet oscillations.

Synthem MII (syn-evaporitic phase) records a restricted, stressed marine evaporitic basin characterized by the record of at least seven gypsum beds. Major salinity changes in a bottom-water stagnation and stratification context are recorded by episodic gypsum precipitation and fluctuations in foraminifer and nannoplankton assemblages. Especially noticeable is the record of dwarf fauna of planktonic foraminifera, which are related to stressed marine conditions in the water column.

Synthem P (post-evaporitic phase) records a significant increase in foraminifer and nannoplankton diversity representing normal marine conditions as a consequence of the early Pliocene reflooding of the basin in a two-step model. In the first step, paleovalleys carved during the late Messinian are overlain by shallow marine and coastal environments. The second step culminates with open marine conditions in a highstand context.

In the studied composite section (Fig. 12), the following key features are pointed out and related to the Messinian Salinity Crisis:

a) The boundary between the pre-evaporitic synthem MI and the evaporitic synthem MII corresponds to an erosional surface, the intra-Messinian unconformity. This discontinuity formed due to a sea-level fall that followed the highstand recorded by the megasequence of synthem MI. The Messinian reflooding of the area marked the beginning of a new regressive sequence recorded in the evaporitic unit (or synthem MII).

b) The truncation at the top of the oolitic grainstones, representing the Terminal Carbonate Complex, is a key feature well represented in the study area. The absence of the Lago-Mare

unit over the evaporitic one can be explained by the fact that it was not deposited in this area, but the possibility cannot be excluded that it was removed by the heavy erosion associated with the end-Messinian unconformity.

c) The end-Messinian unconformity represents a major stratigraphic boundary separating the evaporitic synthem MII from the post-evaporitic one (synthem P). In the study area, this unconformity corresponds to the truncation surface at the San Miguel paleovalley. This paleovalley records the major sea-level fall at the end of the Messinian.

Acknowledgements

This paper was written in the context of the Paleoenvironmental Changes research group (University of Alicante) and supported by project GRE14-05 (University of Alicante). The authors wish to thank Dr. Juan C. Braga and an anonymous referee for their valuable suggestions and critical comments, which have improved the quality of this paper. Thanks are extended to our colleague and grandmaster Alfonso Yébenes for his valuable insights and recommendations. Thanks also to Christine Laurin for revising the English.

References

Aguirre, J., Sánchez-Almazo, I. M., 2004. The Messinian post-evaporitic deposits of the Gafares area (Almería-Níjar basin, SE Spain). A new view of the "Lago-Mare" facies. Sediment. Geol. 168(1), 71–95.

Alfaro, P., Delgado, J., Estévez, A., Molina, J.M., Moretti, M., Soria, J.M., 2002. Liquefaction and fluidization structures in Messinian storm deposits (Bajo Segura basin, Betic Cordillera, southern Spain). Int. J. Earth Sci. – Geol. Rundsch. 91, 505–513.

Aubry, M. P., 1992. Late paleogene calcareous nannoplankton evolution: a tale of climatic deterioration, in: Prothero, D. R. and Berggren, W. A. (Eds.), Eocene-Oligocene Climatic and Biotic Evolution. Princeton University Press, pp. 272–309.

Backman, J., Raffi, I., 1997. Calibration of Miocene nannofossil events to orbitally-tuned cyclostratigraphies from Ceara Rise, in: Shackleton, N.J., Curry, W.B., Richter, C., Bralower, T.J. (Eds.), Proc. ODP, Sci. Res. 154, 83–99.

Bassetti, M. A., Miculan, P., Sierro, F. J., 2006. Evolution of depositional environments after the end of Messinian Salinity Crisis in Níjar basin (SE Betic Cordillera). Sediment. Geol. 188, 279–295.

Boltovskoy, E., Wright, R., 2013. Recent foraminifera. Springer Science & Business Media.

Bourillot, R., Vennin, E., Rouchy, J. M., Blanc-Valleron, M. M., Caruso, A., Durlet, C., 2010. The end of the Messinian Salinity Crisis in the western Mediterranean: Insights from the carbonate platforms of south-eastern Spain. Sediment. Geol. 229(4), 224–253.

Braga, J. C., Martín, J. M. Riding, R., Aguirre, J., Sánchez-Almazo, I. M., Dinarès-Turell, J., 2006. Testing models for the Messinian salinity crisis: The Messinian record in Almería, SE Spain. Sediment. Geol. 188, 131–154.

Braga, J.C., Martín, J.M., Riding, R., 1995. Controls on microbial dome fabric development along a carbonate-siliciclastic shelf basin transect, Miocene, SE Spain. Palaios 10, 347–361.

Brenchley, P.J., Pickerill, R.K., Stromberg, S.G. 1993. The role of wave reworking on the architecture of storm sandstone facies, Bell Island Group (Lower Ordovician), eastern Newfoundland. Sediment. 40, 359–382.

Caracuel, J.E., Corbí, H., Giannetti, A., Monaco, P., Soria, J.M., Tent-Manclús, J.E., Yébenes, A., 2011. Paleoenvironmental changes during the Late Miocene (Messinian)-Pliocene transition: sedimentological and ichnological evidence. Palaios 26, 754-766.

Caracuel, J. E., Soria, J. M., Yébenes, A. 2004. Early Pliocene transgressive coastal lags (Bajo Segura Basin, Spain): a marker of the flooding after the Messinian salinity crisis. Sediment. Geol. 169, 121–128.

Castradori, D., 1998. Calcareous nannofossils in the basal Zanclean of the Eastern Mediterranean Sea: remarks on paleoceanography and sapropel formation, in: Procedings-ocean drilling program scientific results. National Science Foundation, pp 113–124.

Cheel, R.J., 1991. Grain fabric in hummocky cross-stratified storm beds: genetic implications. J. Sed. Petrol. 61, 102–110.

CIESM, 2008. In: Briand, F. (Ed.), The Messinian Salinity Crisis from Mega-deposits to Microbiology — A Consensus Report. CIESM Workshop Monographs, vol. 33. Monaco, 168 pp.

Clauzon, G., Suc, J. P., Do Couto, D., Jouannic, G., Melinte-Dobrinescu, M. C., Jolivet, L., ... & Martinell, J., 2015. New insights on the Sorbas Basin (SE Spain): the onshore reference of the Messinian Salinity Crisis. Mar. Petrol. Geo. 66, 71–100.

Clauzon, G., Suc, J.P., Gautier, F., Berger, A., Loutre, M.F., 1996. Alternate interpretation of the Messinian salinity crisis: Controversy resolved?. Geology 24, 4, 363–366.

Cramp, A., O'Sullivan, G., 1999. Neogene sapropels in the Mediterranean: a review. Mar. Geol. 153(1), 11–28.

Cita, M. B., Wright, R .C., Ryan, W. B. F., Longinelli, A., 1978. Messinian paleoenvironments. In: Init. Rep. DSDP, 42A, pp. 1003–1035.

Cita, M. B., Gartner, S., 1973. The stratotype Zanclean foraminiferal and nannofossil biostratigraphy. Riv. Ital. Paleontol. 79, 503–558.

Corbí, H., Lancis, C., García-García, F., Pina, J. A., Soria, J. M., Tent-Manclús, J. E., Viseras, C., 2012. Updating the marine biostratigraphy of the Granada Basin (central Betic Cordillera). Insight for the Late Miocene palaeogeographic evolution of the Atlantic–Mediterranean seaway. Geobios 45(3), 249–263.

Corbí, H., 2010. Los foraminíferos de la cuenca neógena del Bajo Segura (sureste de España): bioestratigrafía y cambios paleoambientales en relación con la Crisis de salinidad del Mediterráneo. PhD Thesis Universidad de Alicante.

Debenay, J. P., Guillou, J. J., Redois, F., Geslin, E., 2000. Distribution trends of foraminiferal assemblages in paralic environments, in: Ronald, E. (Ed.), Environ. Micropaleontol. Springer US., pp. 39–67.

Di Stefano, A., Sturiale, G., 2010. Refinements of calcareous nannofossil biostratigraphy at the Miocene/Pliocene Boundary in the Mediterranean region. Geobios 43(1), 5–20.

Driever, B.W.M., 1988. Calcareous nannofossil biostratigraphy and paleoenvironmental interpretation of the Mediterranean Pliocene. Utrecht Micropal. Bull. 36, 1–245.

Dronkert, H., 1976. Late Miocene evaporites in the Sorbas basin and adjoining areas. Mem. Soc. Geol. Ital. 16, 203–243.

Esteban, M., 1979. Significance of the Upper Miocene coral reefs of the western

Mediterranean. Palaeogeogr. Palaeoclimatol. Palaeoecol. 29, 169–188.

Fisher, W.L., McGowen, J. H., 1967. Depositional systems in the Wilcox of Texas and their relationship to occurrence of oil and gas. Trans. Gulf Coast Ass. Geol. Soc. 17, 105–125.

Fontanier, C., Jorissen, F. J., Licari, L., Alexandre, A., Anschutz, P., Carbonel, P., 2002. Live benthic foraminiferal faunas from the Bay of Biscay: faunal density, composition, and microhabitats. Deep Sea Research Part I: Oceanographic Research Papers. 49, 751–785.

Fortuin, A. R., Krijgsman, W., 2003. The Messinian of the Níjar Basin (SE Spain): sedimentation, depositional environments and paleogeographic evolution. Sediment. Geol. 160(1), 213–242.

Fortuin, A. R., Krijgsman, W., Hilgen, F. J., Sierro, F. J., 2000. Late Miocene Mediterranean desiccation: topography and significance of the 'Salinity Crisis' erosion surface on-land in southeast Spain: Comment. Sediment. Geol. 133(3), 167–174.

Franseen, E. K., Goldstein, R. H., Farr, M. R., 1998. Quantitative controls on location and architecture of carbonate depositional sequences: Upper Miocene, Cabo de Gata region, SE Spain. J. Sediment. Res. 68(2), 283-298.

Garcés, M., Krijgsman, W., Agustí, J., 1998. Chronology of the late Turolian deposits of the Fortuna basin (SE Spain): implications for the Messinian evolution of the eastern Betics. Earth Planet. Sci. Lett. 163(1), 69–81.

García-García, F., Corbí, H., Soria, J.M., Viseras, C., 2011. Architecture analysis of a river flood-dominated delta during an overall sea-level rise (early Pliocene, SE Spain). Sediment. Geol. 237, 102–113.

Haq, B. U., Worsley, T. R., Burckle, L. H., Douglas, R. G., Keigwin, L. D., Opdyke, N. D., ...,Woodruff, F., 1980. Late Miocene marine carbon-isotopic shift and synchroneity of some phytoplanktonic biostratigraphic events. Geology 8, 427–431.

Hsü, K.J., Montadert, J., L., Bernoulli, F., Cita, M. B., Erickson, A., Farrison, R. E. Kidd, R. B., MeliËres, F., Müller, C., Wright, R., 1977. History of the Messinian salinity crisis. Nature 267, 399–403.

Hsü¸, K. J., Cita, M. B., Ryan, W. B. F., 1973. The origin of the Mediterranean evaporites, in: Init. Rep. DSDP, 13 (II), pp. 1203–1221.

Hilgen, F. J., Bissoli, L., Iaccarino, S., Krijgsman, W., Meijer, R., Negri, A., Villa, G., 2000a. Integrated stratigraphy and astrochronology of the messinian GSSP at Oued Akrech (Atlantic Morocco). Earth Planet. Sci. Lett. 182, 237–251.

Hilgen, F.J., Iaccarino, S., Krijgsman, W., Villa, G., Langereis, C.G., Zachariasse, W.J., 2000b. The Global Boundary Stratotype section and Point (GSSP) of the Messinian Stage (uppermost Miocene). Episodes 23, 172–178.

Hilgen, F. J., Krijgsman, W., 1999. Cyclostratigraphy and astrochronology of the Tripoli diatomite formation (pre-evaporite Messinian, Sicily, Italy). Terra Nova 11, 16–22.

Hilgen, F. J., Krijgsman, W., Langereis, C. G., Lourens, L. J., Santerelli, A., Zachariasse, W. J., 1995. Extending the astronomical (polarity) time scale into the Miocene. Earth Planet. Sci. Lett. 136, 495–510.

Hilgen, F.J., 1991. Astronomical calibration of Gauss to Matuyama sapropels in the Mediterranean and implication for the geomagetic polarity time scale. Earth Planet. Sci. Lett. 104, 226–244.

Hüsing, S. K., Kuiper, K. F., Link, W., Hilgen, F. J., Krijgsman, W., 2009. The upper Tortonian–lower Messinian at Monte dei Corvi (Northern Apennines, Italy): completing a Mediterranean reference section for the Tortonian stage. Earth Planet. Sci. Lett. 282(1), 140–157.

Iaccarino, S. M., Premoli-Silva, I., Biolzi, M., Foresi, L.M., Lirer, F., Turco, E., Petrizzo, M.R., 2007. Practical manual of Neogene planktonic foraminifera. International school on planktonic foraminifera, 6th course. Università degli Studi di Perugia, Perugia.

Iaccarino, S. M., Bossio, A., 1999. Paleoenvironment of uppermost Messinian sequences in the Western Mediterranean (Sites 974, 975 and 978), in: Zahn, R., Comas M. C., Klaus, A. (Eds), Proc. Ocean Drill. Progr., Sci. Results, 161, pp. 529–541.

Iaccarino, S. M., Castradori, D., Cita, M. B., Di Stefano, E., Gaboardi, S., McKenzie, J. A., Spezzaferri, S., Sprovieri, R., 1999. The Mio-Pliocene boundary and the significance of the earliest Pliocene flooding in the Mediterranean. Proc. Confer. Neogene Mediterranean Paleoceanography. Mem. Boll. Soc. Geol. It. 54, 109–132.

Jorissen, F. J., 1988. Benthic foraminifera from the Adriatic Sea: principles of phenotypic variation: Utrecht. Micropal. Bull. 37, 1–174.

Kidd, R.B., Cita, M.B., Ryan, W.B.F., 1978. Stratigraphy of eastern Mediterranean sapropel sequences recovered during Leg 42A and their paleoenvironmental significance. Init. Rep. DSDP 42A, 421–443.

Kirschvink, J.L., 1980. The least-square line and plane and analysis of paleomagnetic data. Geophys. J. Astron. Soc. 62, 699–718.

Kouwenhoven, T. J., Van der Zwaan, G. J., 2006. A reconstruction of late Miocene Mediterranean circulation patterns using benthic foraminifera. Palaeogeogr. Palaeoclimatol. Palaeoecol. 238, 373–385.

Krijgsman, W., Meijer, P. T. 2008. Depositional environments of the Mediterranean “Lower Evaporites” of the Messinian salinity crisis: Constraints from quantitative analyses. Marine Geology 253(3), 73–81.

Krijgsman, W., Leewis, M. E, Garcés, M., Kouwenhoven, T. J., Kuiper, K. F., Sierro, F. J., 2006. Tectonic control for evaporite formation in the Eastern Betics (Tortonian; Spain). Sediment. Geol. 188, 155–170.

Krijgsman, W., Fortuin, A. R., Hilgen, F. J., Sierro, F. J. 2001. Astrochronology for the Messinian Sorbas basin (SE Spain) and orbital (precessional) forcing for evaporite cyclicity. Sediment. Geol. 140, 43–60.

Krijgsman, W., Garcés, M., Agustı, J., Raffi, I., Taberner, C., & Zachariasse, W. J., 2000. The 'Tortonian salinity crisis' of the eastern Betics (Spain). Earth Planet. Sc. Lett. 181(4), 497-511.

Krijgsman, W., Hilgen, F. J., Raffi, I., Sierro, F. J., Wilson, D. S. 1999. Chronology, causes and progression of the Messinian salinity crisis. Nature 400, 652–655.

Lancis, C., Tent-Manclús, J.E., Soria, J. M., Caracuel, J. E., Corbí, H., Dinarès-Turell, J., Estévez, A., Yébenes, A., 2010. Nannoplankton biostratigraphic calibration of the evaporitic events in the Neogene Fortuna Basin (SE Spain). Geobios 43, 201–217.

Lancis, C., Flores, J.A., 2006. A new biostratigraphically significant calcareous nannofossil species in the Early Pliocene of the Mediterranean. Micropaleontol. 52, 477–481.

Lancis, C., 1998. El nanoplancton calcáreo de las cuencas neógenas orientales de la Cordillera Bética. Ph.D. Thesis, Univ. Alicante, Spain.

Lourens, L. J., Hilgen, F. J., Laskar, J., Shackleton, N. J., Wilson, D., 2004. The Neogene period, in: Gradstein, F., Ogg, J. et al. (Eds.), A Geologic Time Scale. Cambridge University Press, pp. 409–440.

Lu, F. H., 2006. Lithofacies and water-body record of Messinian evaporites in Níjar Basin, SE Spain. Sediment. Geol. 188, 115–130.

Lugli S., Manzi V., Roveri M., Schreiber B. C., 2010. The Primary Lower Gypsum in the

Mediterranean: A new facies interpretation for the first stage of the Messinian salinity crisis. Palaeogeogr. Palaeoclimatol. Palaeoecol. 297 (1), 83–99.

Manzi, V., Gennari, R., Hilgen, F., Krijgsman, W., Lugli, S., Roveri, M., Sierro, F.J., 2013. Age refinement of the Messinian salinity crisis onset in the Mediterranean. Terra Nova 25, 315–322.

Martínez del Olmo, W., 2011. El Arrecife Messiniense del sondeo Torrevieja Marino C-1 desde las líneas sísmicas (SE. de España). Rev. Soc. Geol. España, 24(3), 173–186.

Martínez del Olmo, W., Serrano Oñate, A., 2000. Secuencias de depósito en el Neógeno de la Cuenca del Mar Menor (Alicante-Murcia, SE de España). Geotemas 1(2), 243–246.

Martín, J.M., Braga, J.C., Sánchez-Almazo, I.M., 1999. The Messinian record of the outcropping marginal Alboran basin deposits: significance and implications. In: Zahn, R., Comas, M.C., Klaus, A. (Eds.), Proc. ODP, 161, 543–551.

Martín, J., Braga, J. C., 1994. Messinian events in the Sorbas Basin in southeastern Spain and their implications in the recent history of the Mediterranean. Sediment. Geol. 90(3), 257-268.

Martín, J.M., Braga, J.C., Riding, R., 1993. Siliciclastic stromatolites and thrombolites, Late Miocene, S.E. Spain. J. Sediment. Petrol. 63, 131–139.

Martini, E., 1971, Standard Tertiary and Quaternary Calcareous Nannoplankton Zonation, in Farinacci, A. (Ed.), Proceedings of the II Planktonic Conference. Roma , 1970, Tecnoscienza, pp. 739–785.

Michalzik, D., 1996. Lithofacies, diagenetic spectra and sedimentary cycles of Messinian (Late Miocene) evaporites in SE Spain. Sediment. Geol. 106, 203–222.

Michalzik, D., Elbracht, J., Mauthe, F., Reinhold, C., Schneider, B., 1993. Messinian facies relations in the San Miguel de Salinas Basin, SE Spain. Z. Deutsch Geol. Ges. 144, 352–369.

Montadert, L., Letouzey, J., Mauffret, A. 1978. Messinian event: seismic evidence. Initial Rep. Deep Sea Drill. Proj. 42 (Part 1), 1037–1050.

Montenat, Ch., 1990. Les bassins nèogenes du domaine bètique oriental (Espagne). Tectonique et sèdimentation dans un couloir de décrochement. Premiere partie: Ètude règionale. Documents et Travaux I.G.A.L. 12-13, 1–392.

Morigi, C., Negri, A., Giunta, S., Kottwenhoven, T., Krijgsman, W., Blanc-Valleron, M. M., Orszag-Sperber, F., Rouchy, J. M., 2007. Integrated quantitative biostratigraphy of the latest Tortonian-early Messinian Pissouri section (Cyprus): An evaluation of calcareous plankton bioevents. Geobios 40, 267–279.

Müller, C., 1990. Nannoplankton biostratigraphy and paleoenvironmental interpretations from the Tyrrhenian Sea, ODP Leg 107 (Western Mediterranean). In: Kastens, K. A., Mascle, J. et al., (Eds.), Proc. ODP, Sci. Result.,107, pp. 495–511.

Müller, C., 1978. Neogene calcareous nannofossils from the Mediterranean- Leg 42A of the Deep Sea Drilling Project. In: Hsü, K. J., Montadert L. et al. (Eds.), Init. Rep. DSDP, 42, pp. 727-751.

Münch, Ph, Cornée, J.J., Féraud, G., Saint Martin, J.P., Ferrandini, M., García, F., Conesa, G., Roger, S., Moullade, M., 2006. Precise 40Ar/39Ar dating of volcanic tuffs within the upper Messinian sequences in the Melilla carbonate complex (NE Morocco): implications for the Messinian salinity crisis. Int. J. of Earth Sci. 95, 491–503

Murray, J. W., 1991. Ecology and paleoecology of benthic foraminifera. N. Y. Longman Scientific and Technical, New York.

Negri, A., Giunta, S., Hilgen, F., Krijgsman, W. Vai, G. B. 1999., Calcareous nannofossil biostratigraphy of the M. del Casino section (northern Apennines, Italy) and paleoceanographic conditions at times of Late Miocene sapropel formation. Mar. Micropaleontol. 36, 13–30.

Ochoa, D., Sierro, F. J., Lofi, J., Maillard, A., Flores, J. A., Suárez, M., 2015. Synchronous onset of the Messinian evaporite precipitation: First Mediterranean offshore evidence. Earth Planet. Sc. Lett. 427, 112-124.

Okada, H., Bukry, D., 1980. Supplementary modification and introduction of code numbers to the low-latitude coccolith biostratigraphic zonation. Mar. Micropaleontol. 5, 321–325.

Ortí-Cabo F., Shearman, F. J., 1977. Estructuras y fabricas deposicionales en las evaporitas del mioceno superior (Messiniense) de San Miguel de Salinas (Alicante, España). Rev. Inst. Inv. Geol. Dip. Prov. Barcelona 32, 5–53.

Orszag-Sperber, F., 2006. Changing perspectives in the concept of “Lago-Mare” in Mediterranean Late Miocene evolution. Sediment. Geol. 188–189, 259–277.

Playà, E., Ortí, F., Rosell, L., 2000. Marine to non-marine sedimentation in the upper Miocene evaporites of the Eastern Betics, SE Spain: sedimentological and geochemical evidence. Sediment. Geol. 133, 135–166.

Raffi, I., Backman, J., Fornaciari, E., Pälike, H., Rio, D., Lourens, L. Hilgen, F., 2006. A review of calcareous nannofossil astrobiochronology encompassing the past 25 million years. Quat. Sci. Rev. 25, 3113–3137.

Raffi, I., Mozzato, C., Fornaciari, E., Hilgen, F. J., Rio, D., 2003. Late Miocene calcareaous nannofossil biostratigraphy and astrobiochronology for the Mediterranean region. Micropaleontol. 49, 1–26.

Riding, R., Braga, J.C., Martín, J.M., 2000. Late Miocene Mediterranean desiccation: topography and significance of the 'Salinity Crisis' erosion surface on-land in southeast Spain: reply. Sediment. Geol. 133, 175–184.

Riding, R., Braga, J. C., Martín, J. M., 1999. Late Miocene Mediterranean desiccation: topography and significance of the Salinity Crisis' erosion surface on-land in southeast Spain. Sediment. Geol., 123(1), 1-7.

Riding, R., Braga, J. C., Martín, J. M., Sánchez-Almazo, I. M., 1998. Mediterranean Messinian Salinity Crisis: constraints from a coeval marginal basin, Sorbas, southeastern Spain. Mar. Geol. 146, 1–20.

Riding, R., Braga, J.C., Martín, J.M., 1991. Oolite stromatolites and thrombolites, Miocene, Spain: analogues of Recent giant Bahamian examples. Sediment. Geol. 71, 121–127.

Rosell, L., Ortí-Cabo, F., García-Veigas, J., 1994. Geoquímica del estroncio en los yesos messinienses de la cuenca de San Miguel de Salinas (Alicante). Geogaceta 15, 82–85.

Rouchy, J. M., Caruso, A., 2006. The Messinian salinity crisis in the Mediterranean basin: A reassessment of the data and an integrated scenario. Sediment. Geol. 188-189, 35–67.

Roveri, M., Flecker, R., Krijgsman, W., Lofi, J., Lugli, S., Manzi, V., ..., Stoica, M., 2014. The Messinian Salinity Crisis: Past and future of a great challenge for marine sciences. Mar. Geol. 352, 25–58.

Roveri, M., Gennari, R., Lugli, S., Manzi, V., 2009. The terminal carbonate complex: the record of sea-level changes during the Messinian salinity crisis. Geoacta 8, 57–71.

Roveri, M., Lugli, S., Manzi, V., & Schreiber, B. C., 2008. The Messinian Sicilian stratigraphy revisited: new insights for the Messinian salinity crisis. Terra Nova 20(6), 483-488.

Roveri, M., Bassetti, M. A., Lucchi, F. R., 2001. The Mediterranean Messinian salinity crisis: an Apennine foredeep perspective. Sediment. Geol. 140(3), 201-214.

Sánchez-Almazo, I. M., Braga, J. C., Dinarès-Turell, J., Martín, J. M., Spiro, B., 2007. Palaeoceanographic controls on reef deposition: the Messinian Cariatiz reef (Sorbas Basin, Almería, SE Spain). Sediment. 54(3), 637-660.

Shannon, C. E., Weaver, W., 1949. The mathematical theory of communication. Urbana, Univ. Illinois Press.

Shearman, D. J., Ortí-Cabo, F., 1976. Upper Miocene gypsum: San Miguel de Salinas, SE Spain. Mem. Soc. Geol. Ital. 16, 327–340.

Sierro, F. J., Flores, J. A., Frances, G., Vazquez, A., Utrilla, R., Zamarreno, I. Erlenkeuser, H., Barcena, M. A. , 2003. Orbitally-controlled oscillations in planktic communities and cyclic changes in western Mediterranean hydrography during the Messinian. Palaeogeogr. Palaeoclimatol. Palaeoecol. 190, 289–316.

Sierro, F. J., Hilgen, F. J., Krijgsman, W., Flores, J. A., 2001. The Abad composite (SE Spain): a Messinian reference section for the Mediterranean and the APTS. Palaeogeogr. Palaeoclimatol. Palaeoecol. 168(1), 141–169.

Sierro, F. J., Flores, J. A., Zamarreno, I., Vazquez, A., Utrilla, R., Frances, G. Hilgen, F. J., Krijgsman, W., 1999. Messinian pre-evaporite sapropels and procession-induced oscillations in western Mediterranean climate. Mar. Geol. 153, 137–146.

Sierro, F. J., Flores, J. A., Civis, J., Delgado, J. A. G., Francés, G., 1993. Late Miocene Globorotaliid event-stratigraphy and biogeography in the Ne-Atlantic and Mediterranean. Mar. Micropaleontol. 21, 143–168.

Sierro, F. J., 1985. The Replacement of the Globorotalia menardii group by the Globorotalia miotumida group - an aid to recognizing the Tortonian-Messinian boundary in the Mediterranean and adjacent Atlantic. Mar. Micropaleontol. 9, 525–535.

Sloss, L. L., 1969. Evaporite deposition from layered solutions. AAPG Bulletin, 53(4), 776–789.

Soria, J. M., Giannetti, A., Monaco, P., Corbí, H., García-Ramos, D., Viseras, C., 2014. Cyclically-arranged, storm-controlled, prograding lithosomes in Messinian terrigenous shelves (Bajo Segura Basin, western Mediterranean). Sediment. Geol. 310, 1-15.

Soria, J. M., Caracuel, J. E., Corbí, H., Dinarès-Turell, J., Lancis, C., Tent-Manclús, J. E., Viseras, C., Yébenes, A., 2008a. The Messinian-early Pliocene stratigraphic record in the southern Bajo Segura Basin (Betic Cordillera, Spain): Implications for the Mediterranean salinity crisis. Sediment. Geol. 203, 267–288.

Soria, J. M., Caracuel, J. E., Corbí, H., Dinarès-Turell, J., Lancis, C., Tent-Manclús, J. E., Yébenes, A., 2008b. The Bajo Segura Basin (SE Spain): implications for the Messinian Salinity Crisis in the Mediterranean margins. Stratigraphy 5, 259–265.

Soria, J. M., Caracuel, J. E., Corbí, H., Yébenes, A., 2007. La sedimentación de afinidad Lago Mare (Messiniense) y la transgresión del Plioceno en Alicante (Cuenca del Bajo Segura). Geogaceta 41, 219–222.

Soria, J. M., Caracuel, J. E., Yébenes, A., Fernández, J., Viseras, C., 2005. The stratigraphic record of the Messinian salinity crisis in the northern margin of the Bajo Segura Basin (SE Spain): Sediment. Geol. 179, 225–247.

Vail, Peter R., R. M. Mitchum, and S. Thompson, 1977. Seismic stratigraphy—applications to hydrocarbon exploration. AAPG Mem. 26, 49–212.

Van de Poel, H.M., 1992. Foraminiferal biostratigraphy and palaeoenvironments of the

Miocene–Pliocene Carboneras–Nijar Basin (SE Spain). Scr. Geol. 102, 1–32

Van der Zwaan, G. J., Jorissen, F. J., Destigter, H. C., 1990. The Depth Dependency of Planktonic Benthic Foraminiferal Ratios - Constraints and Applications. Mar. Geol. 95, 1–16.

Van der Zwaan, G. J., 1982. Paleoecology of Late Miocene Mediterraean foraminifera. Utrecht Micropal. Bull. 25, 1–202.

Wade, B. S., Bown, P. R., 2006. Calcareous nannofossils in extreme environments: The Messinian Salinity Crisis, Polemi Basin, Cyprus. Palaeogeogr. Palaeoclimatol. Palaeoecol. 233, 271–286.

Walker, R.G., 1979. Shallow marine sands, in: Walker, R.G. (Ed.), Facies Models. Geoscience Canada, Reprint Series, vol. 1, pp. 75–89.

Wright, R., 1978. Neogene paleobathymetry of the Mediterranean based on benthic foraminifers from DSDP Leg 42A. Init. Repts. DSDP 42, 837–847.

Young, J. R., 1994. A summary chart of Neogene nannofossil magnetobiostratigraphy. J.Nannoplankton Res. 16, 21–27.

Zaninetti, L., 1984. Les foraminifers du salin de Bras del Port (Santa Pola, Espagne) avec remarques sur le distribution des ostracodes. Rev. Inv. Geol. 38/39, 123–38.

Zaninetti, L., 1982. Les foraminifères des marais salants de Salin-de-Giraud (sud de la France): milieu de vie et transports dans le salin, comparaison avec les microfaunes marines. Geol. Med. 9, 447–70.

Zijderveld, J. D. A., 1967. A. C. demagnetization of rock: analysis of results, in: Methods in paleomagnetism (Collinson, D.W., Creer, K.M., Run, S. K. (Eds.), Elsevier, Amsterdam, pp. 254–286.

Figure captions

Figure 1. Geological context of the Bajo Segura basin. A) Location of the Betic Cordillera in the western Mediterranean. B) Geological map of the Eastern Betic Cordillera showing the location of the Bajo Segura basin. C) Geological map of the Bajo Segura basin, indicating the position of the San Miguel de Salinas sector.

Figure 2. The San Miguel de Salinas sector. A) Synthetic stratigraphic architecture of the Bajo Segura basin, with the location of the San Miguel de Salinas composite section. B) Geological map of the San Miguel de Salinas sector, with the position of the three study sections. As stated in the sedimentological description, the depositional systems are characterized by the following facies. MIa: alternating gray and brownish laminated marls with sporadically interbedded sandstone beds; MIb: thickening-upward sandstone-dominated beds with sandy marls; MIIa: alternating marls with intercalated sandstones and gypsum beds; MIIb: thickening-upward sandstone-dominated interval evolving gradually into the MIIb(o) system comprising carbonate-dominated grainstones; P0: conglomerates and coarse-grained sandstones; P1: marls with interbedded fine-grained sandstones; P2: sandstone-dominated interval; and P3: red clays and conglomerates representing continental environments.

Figure 3. Stratigraphic framework of the San Miguel de Salinas sector. A) Geometry of the MI, MII, and P synthems. It should be noted that this synthetic stratigraphic architecture shows only the marine Messinian and Pliocene synthems in the San Miguel de Salinas sector (synthem P3, not analyzed in this work, is not represented). B) litho-, bio-, and magnetostratigraphic logs for the three study sections (VGP: virtual geomagnetic pole; solid circles: class A sites; open circles: class B sites; crosses: class C sites); chrons (at the left of the lithological logs) according to the ATNTS 2004 (Astronomically Tuned Neogene Time Scale; Lourens et al., 2004). C) Stereographic projections of the ChRM components of the 26 class A inverse samples before (in situ) and after bedding correction (tilt corrected) are shown (open

symbols indicate projections onto the upper hemisphere), together with the mean direction and statistics. The 95% confidence ellipse is indicated. Statistical information is given (N, number of samples; Dec., declination; Inc., inclination: k Fisher's precision parameter; α95, radius of the 95% confidence cone).

Figure 4. Representative class A tilt-corrected orthogonal demagnetization diagrams from the study sections (sample numbers are referenced with respect to Fig. 3B). The natural remanent magnetization (NRM) intensity and some demagnetization steps are indicated. Open and closed symbols indicate projections onto the upper and lower hemisphere respectively. The computed ChRM direction is shown by a solid line.

Figure 5. Synthem MI (Lo Rufete section). A) General field view of the Lo Rufete section showing the gradual upward evolution from the MIa to the MIb depositional systems; the stacking pattern of the sandstone beds in the MIb system defines three thickening-upward sequences. The sharp surface at the top of the MI synthem corresponds to the intra-Messinian unconformity. Synthem MII overlies this unconformity showing a similar stacking pattern in the sandstone beds; a lower MIIa depositional system (marl dominated) and an upper MIIb (sandstone dominated) system can be differentiated. B) Typical alternation of homogeneous (m) and brownish marls (s), which can be associated to "sapropel" (see discussion in the text) in the MIa depositional system; thin sandstone layers (st) are marked by red lines. C) Sandstone with planar lamination, interpreted as a turbidite (Tb interval) or, alternatively, as a tempestite (planar lamination interval). D) *Thalassinoides* in the sandstone layers. E and F) Hummocky cross-stratification in sandstone beds from the MIb depositional system. G) White stromatolites at the boundary between the MI and MII synthems, in correspondence to the intra-Messinian unconformity. H and I) Large-scale desiccation cracks in the stromatolite bed; orange arrows point to the position of tepees, white arrows indicate polygonal contours of the desiccation cracks.

Figure 6. Synthem MII (A–E: Km16 section; F–H: Canal section). A) Typical laminated, organic-rich marls from the MIIa depositional system. B) Tempestite layer in the laminated marls, showing planar lamination in the lower part and hummocky cross-stratification in the upper part. C) Thin tempestite layer with oscillatory ripples at the top. D) Giant selenitic gypsum in the G1 bed, showing an irregular top and cavities filled by laminated marls. E) Outcrop view of the lower part of the Km16 section, corresponding to the depositional system MIIa, where gypsum beds G1 to G4 alternate with laminated marls. F) Massive and banded selenitic gypsum beds G4 and G5in the Canal section; note the irregular base and the flat top. G) Lateral disappearance of gypsum bed G5 in the laminated marls. Note the evolution from tabular to cluster-like or supercones. Frequent sandy tempestite layers (st) are interbedded. H) Outcrop view of gypsum beds G6 and G7 alternating with laminated marls in the Canal section. Both gypsum beds are composed of branching selenite (see right inset box).

Figure 7. Synthem MII (Km16 section). A) A single tempestite layer showing planar lamination and rip-up mud clasts in the lower part, and hummocky cross-stratification in the upper part. B) Amalgamated tempestite layers from the depositional system MIIb; individual layers are separated by rip-up mud clast-dominated intervals. C) Mixed siliciclastic-carbonate sandstones and oolitic grainstones forming the upper part of the depositional system MIIb(o); multidirectional cross-lamination generated by the migration of small- to medium-scale sand waves are indicative of a shoreface environment. D) Low-angle foreshore lamination at the top of the depositional system MIIb(o).

Figure 8. Synthem P (A–B: Km16 section; C–E: Canal section). A and B) Details of the end-Messinian unconformity in the Km16 section. This unconformity is marked by an intensely bioturbated surface separating MIIb from the P2 depositional systems. C) Basal conglomerate (P0 depositional system) in the Canal section; clast lithology indicates provenance from the underlying MIIb depositional system. D) Planktonic-rich marls with sandstone layers forming

the P1 systems in the Canal section. E) Cyclic arrangement of the P2 system in the Km16 section. Bipartite cycles (white arrows) are defined by a regular alternation of silts and indurated fine-grained sandstones. F) *Thalassinoides* in the P2 cycles. G) Silt/sandstone bipartite cycles of the P2 system in the Canal section. Note the similar cyclic arrangement with respect to the Km16 section (image E).

Figure 9. Foraminiferal and nannoplankton data of the Lo Rufete section used for paleoenvironmental reconstruction; H (s): Shannon-Weaver index (Shannon and Weaver, 1949); %P: planktonic foraminifer ratio with regard to the whole of the assemblage; warm-oligotrophic/cold-eutrophic: ratio between warm-oligotrophic water (black column) and cold-eutrophic water planktonic foraminifera. It should be noted that dwarf asteroliths have not been included because of their scarce presence in the nannoplankton assemblage.

Figure 10. Foraminiferal and nannoplankton data of the Km16 section used for paleoenvironmental reconstruction; H (s): Shannon-Weaver index; %P: planktonic foraminifer ratio with regard to the whole of the assemblage; warm-oligotrophic/cold-eutrophic: ratio between warm-oligotrophic water (black column) and cold- eutrophic water planktonic foraminifera.

Figure 11. Foraminiferal and nannoplankton data of the El Canal section used for paleoenvironmental reconstruction; specific richness: H (s): Shannon-Weaver index; %P: planktonic foraminifera ratio regard to the whole of the assemblage; Warm-oligotrophic/cold-eutrophic: ratio between warm-oligotrophic water (black column) and cold- eutrophic water planktonic foraminifera.

Figure 12. Synthetic scheme of the stratigraphic and paleoenvironmental evolution from the San Miguel de Salinas composite section.

Figure 1

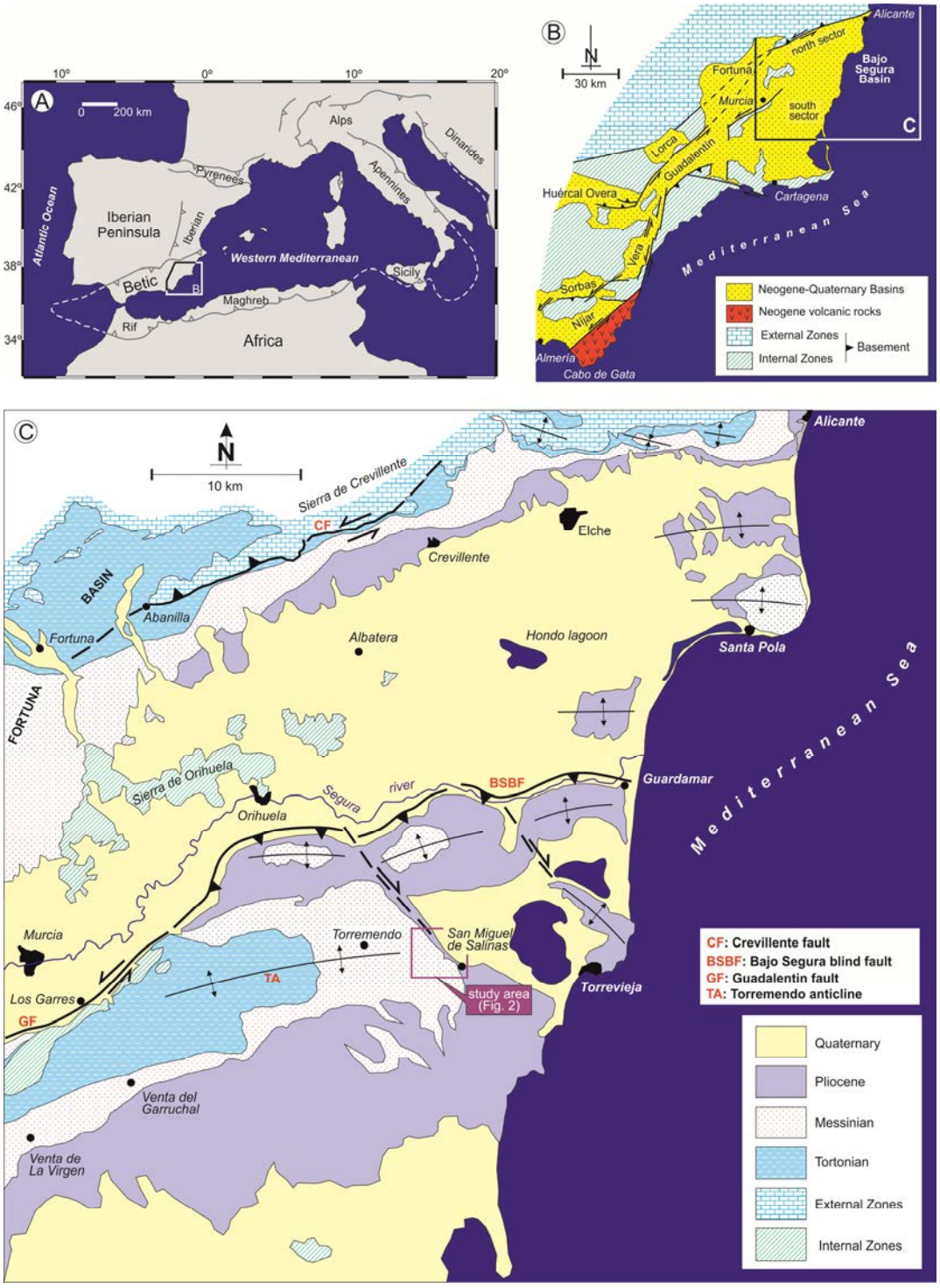

Figure 2

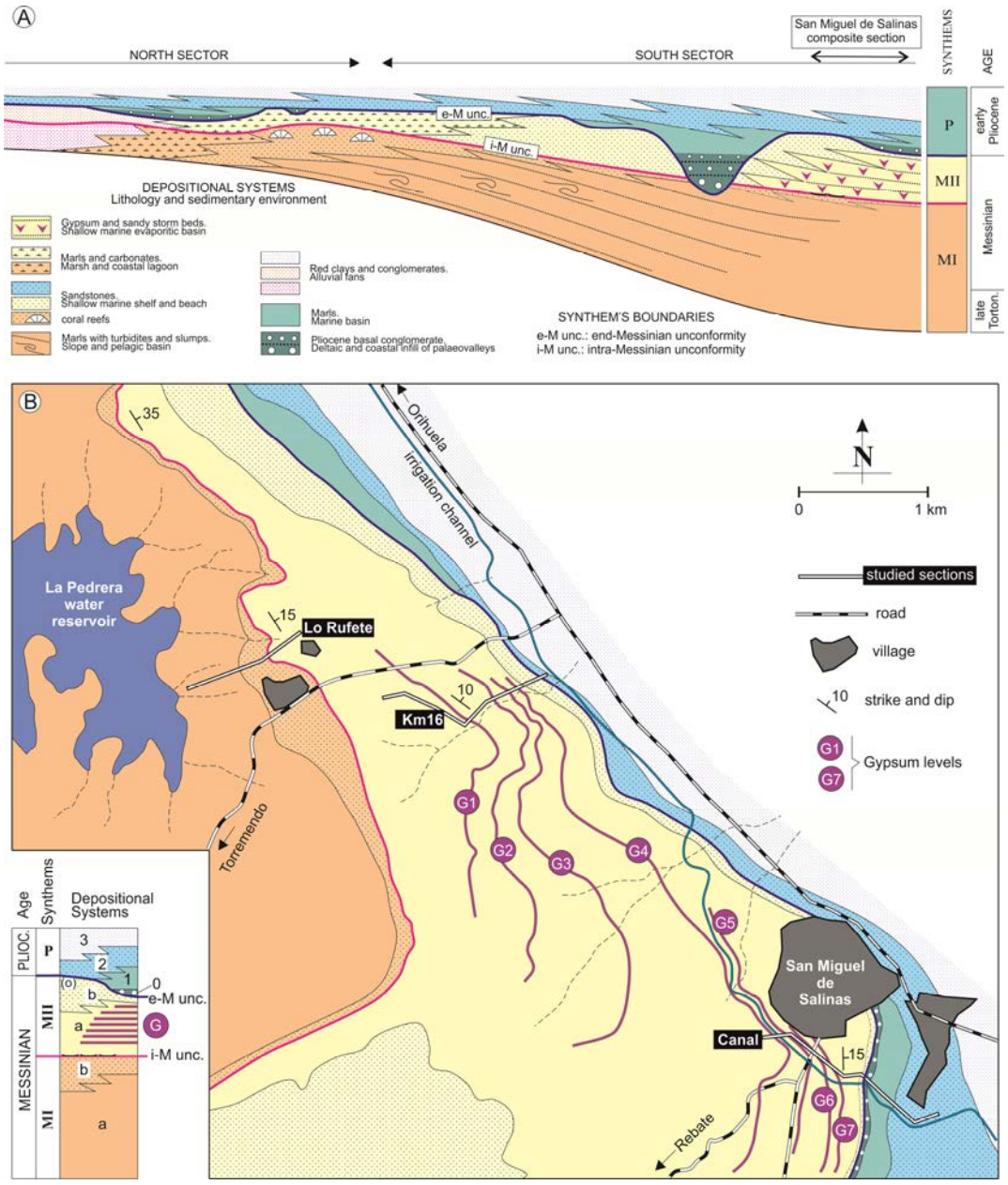

Figure 3

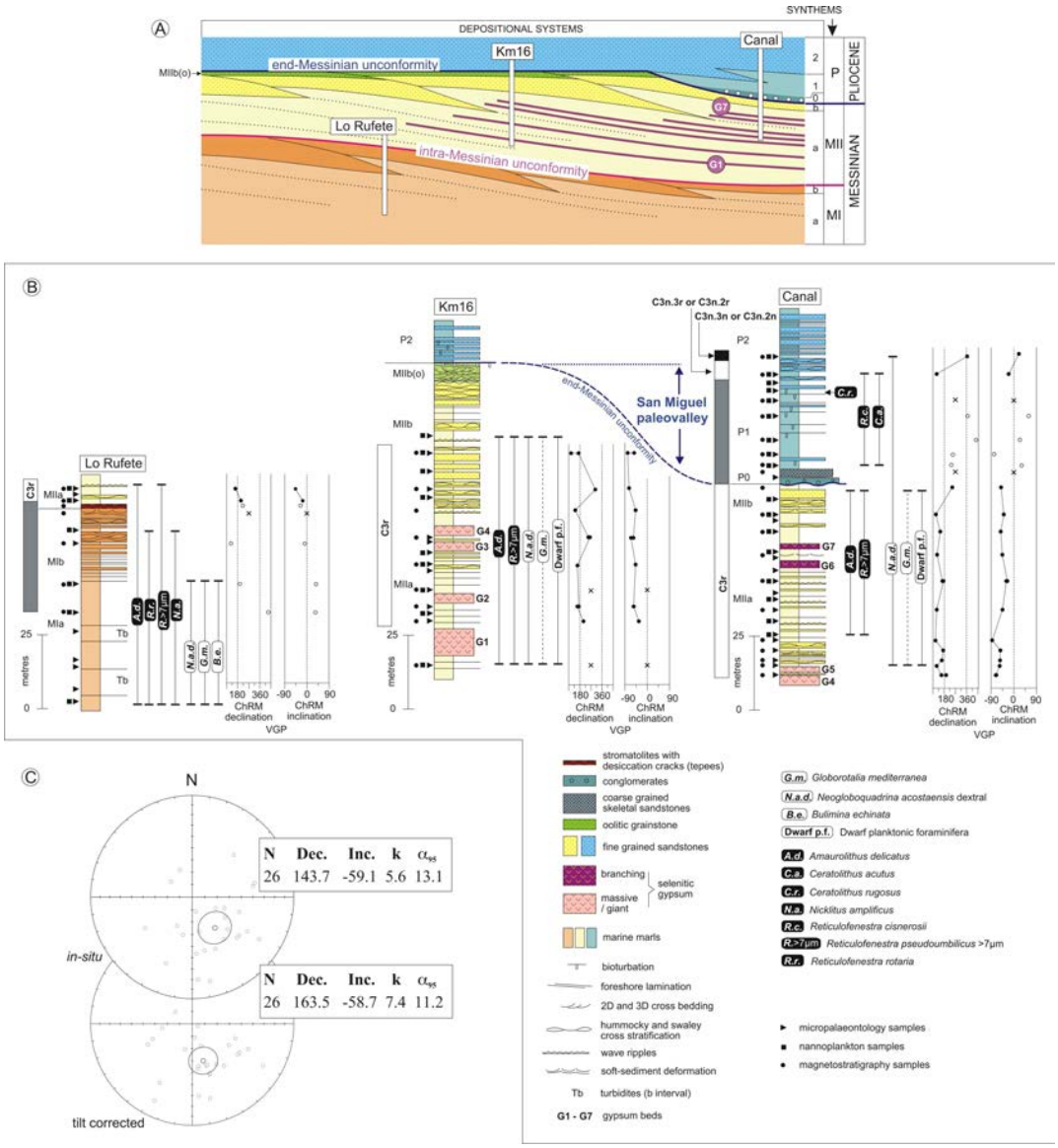

Figure 4

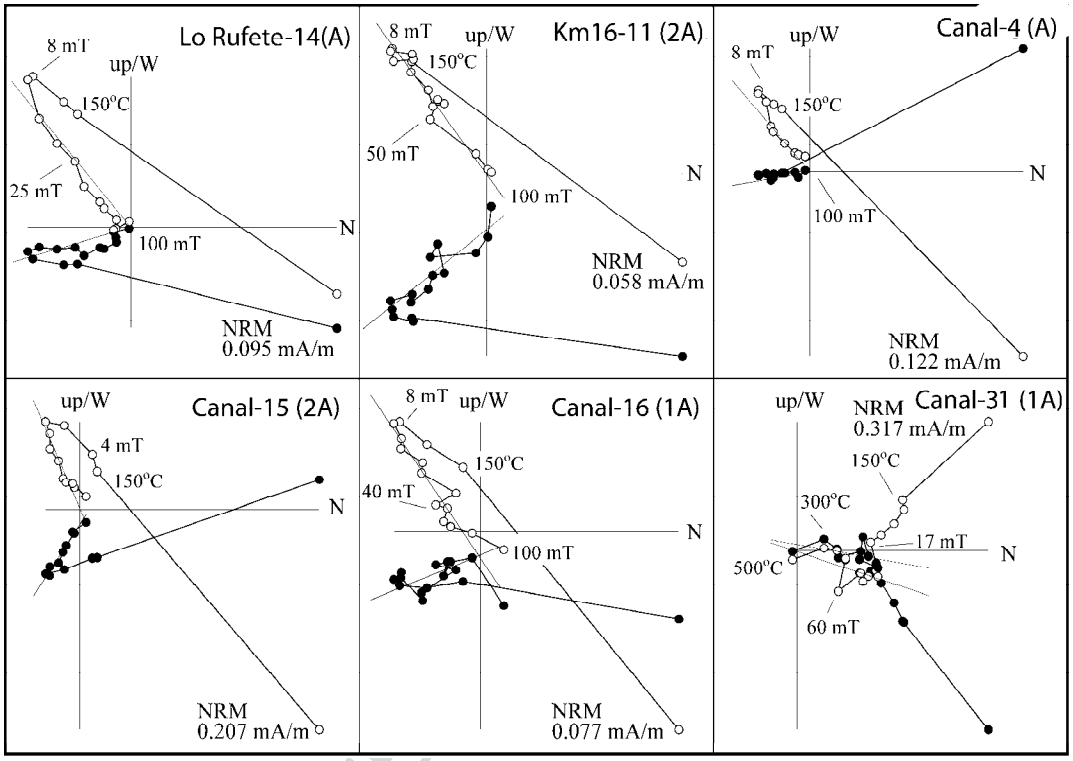

Figure 5

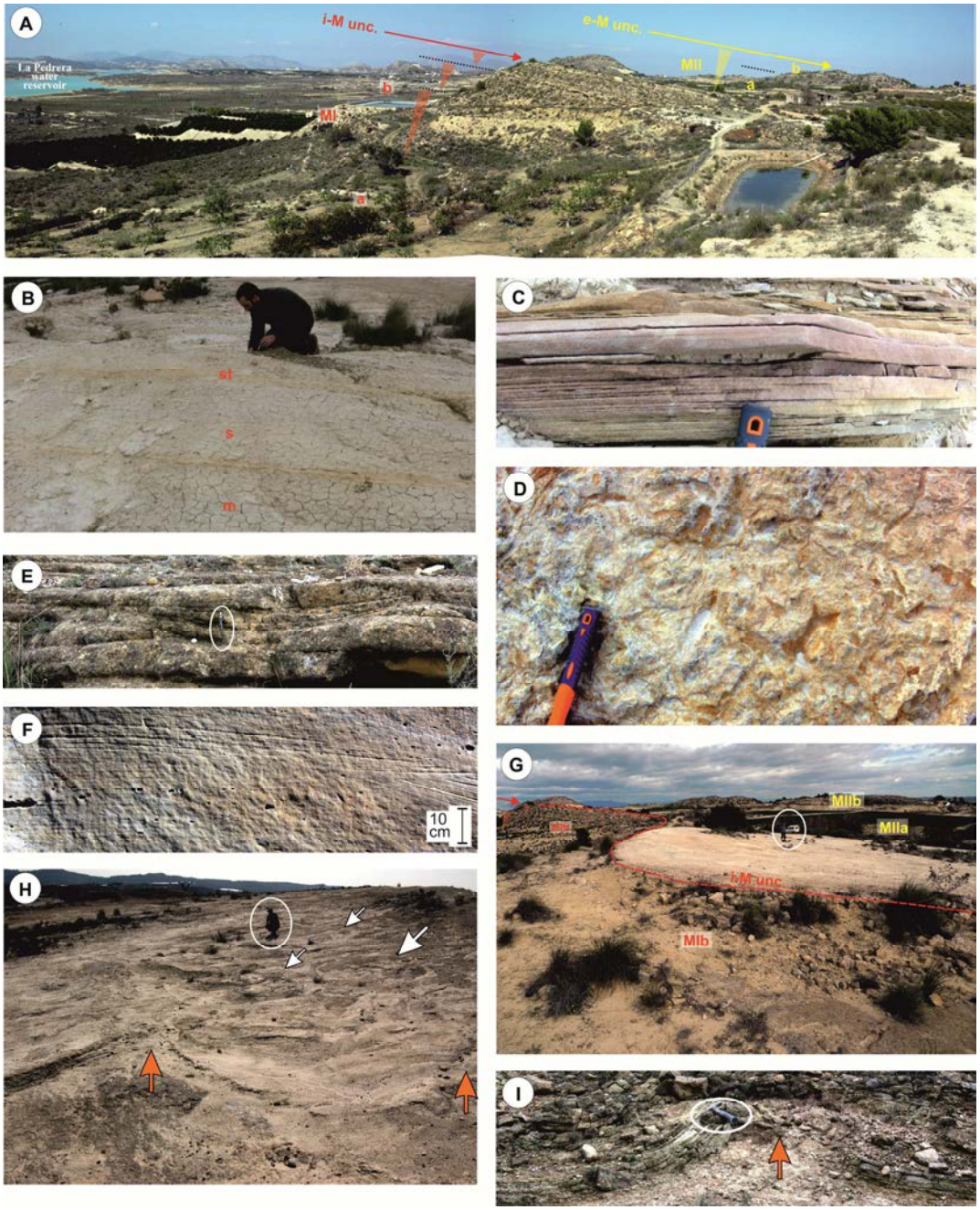

Figure 6

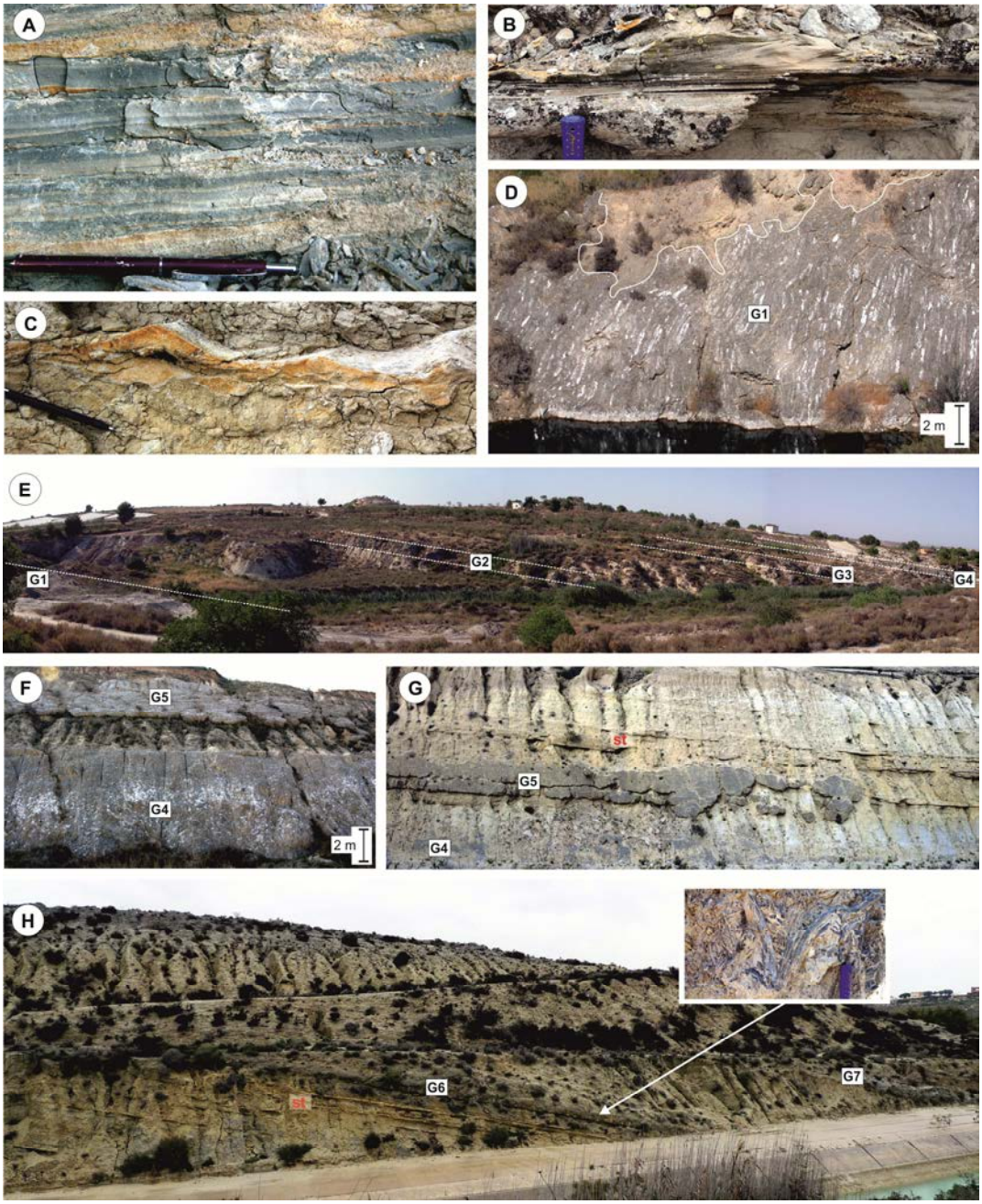

Figure 7

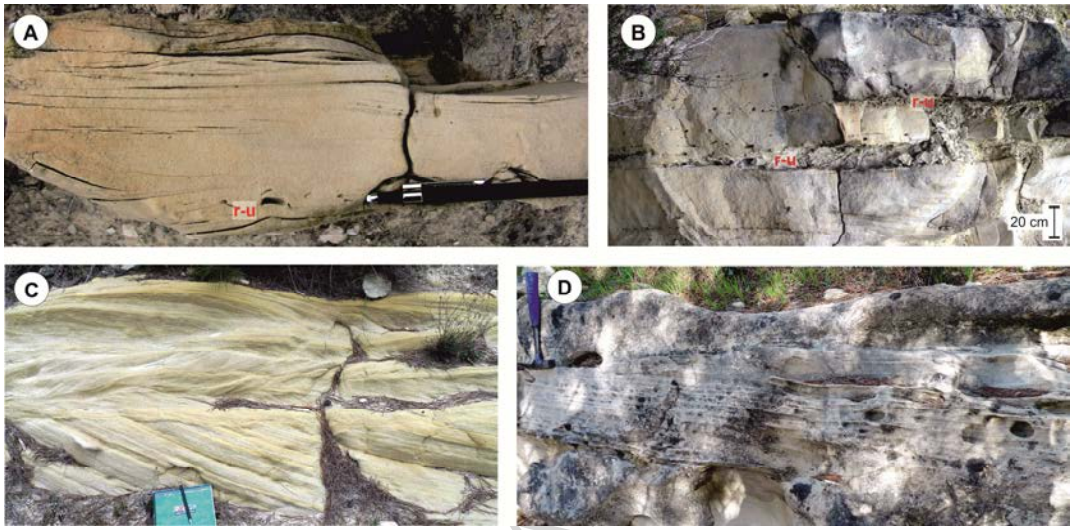

Figure 8

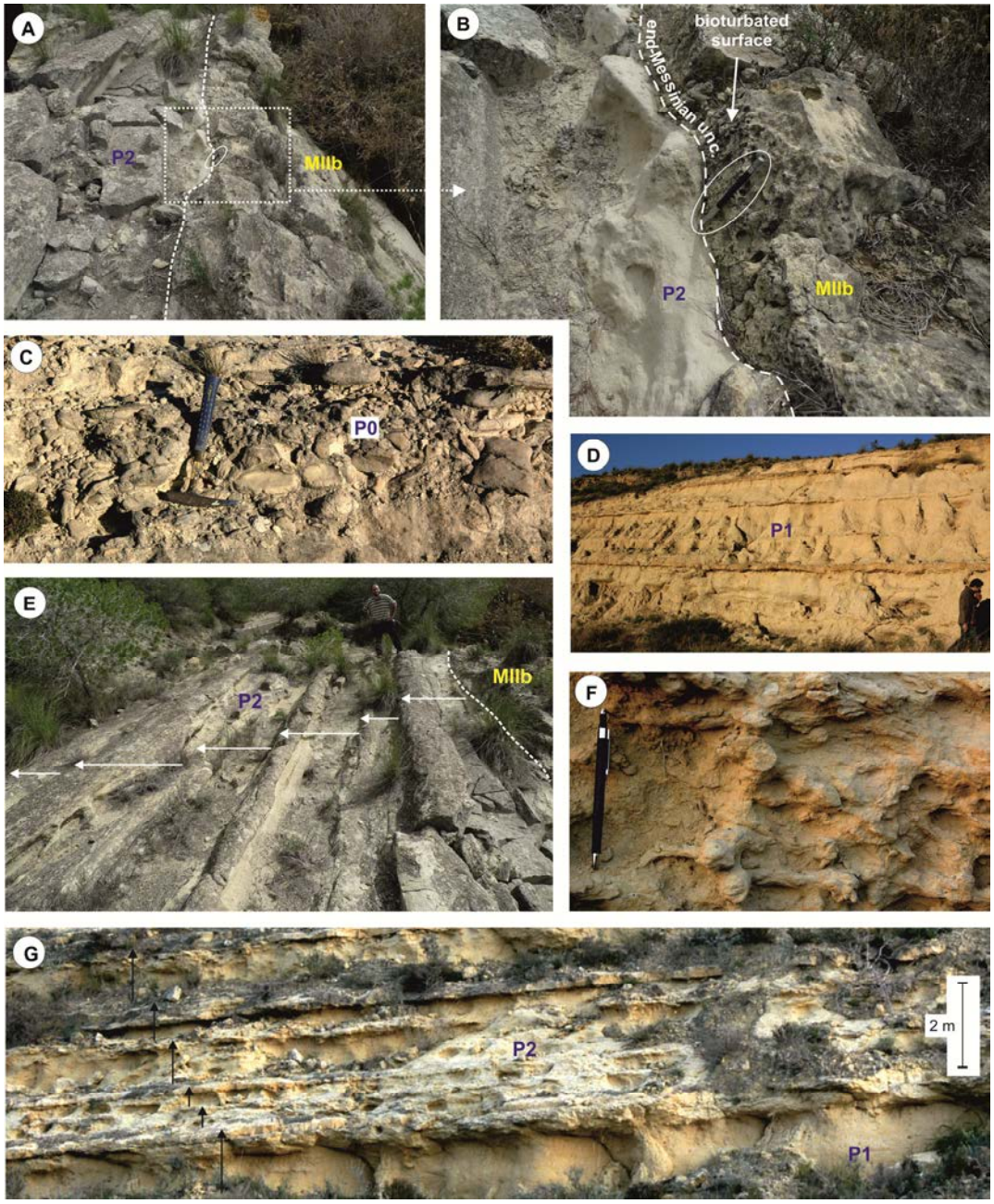

Figure 9

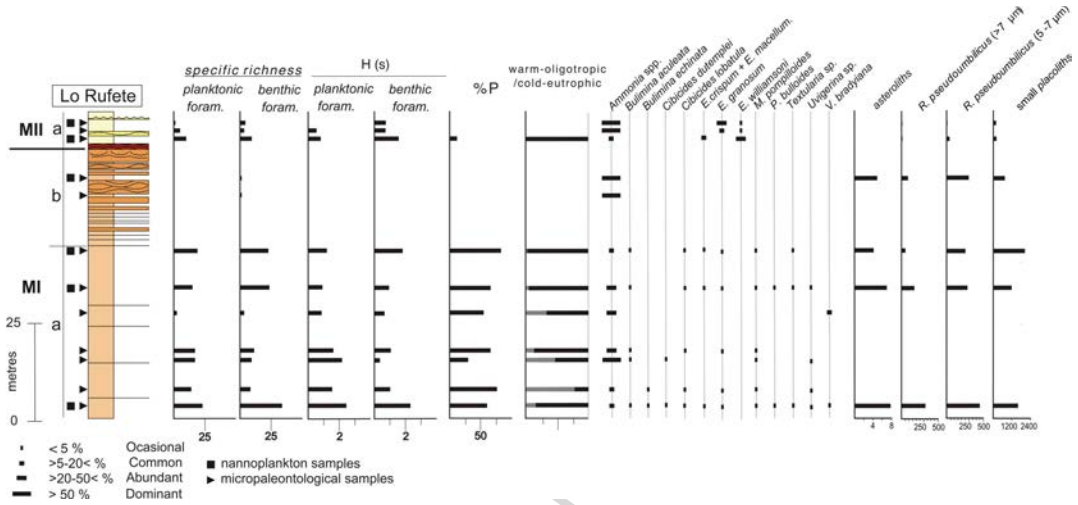

Figure 10

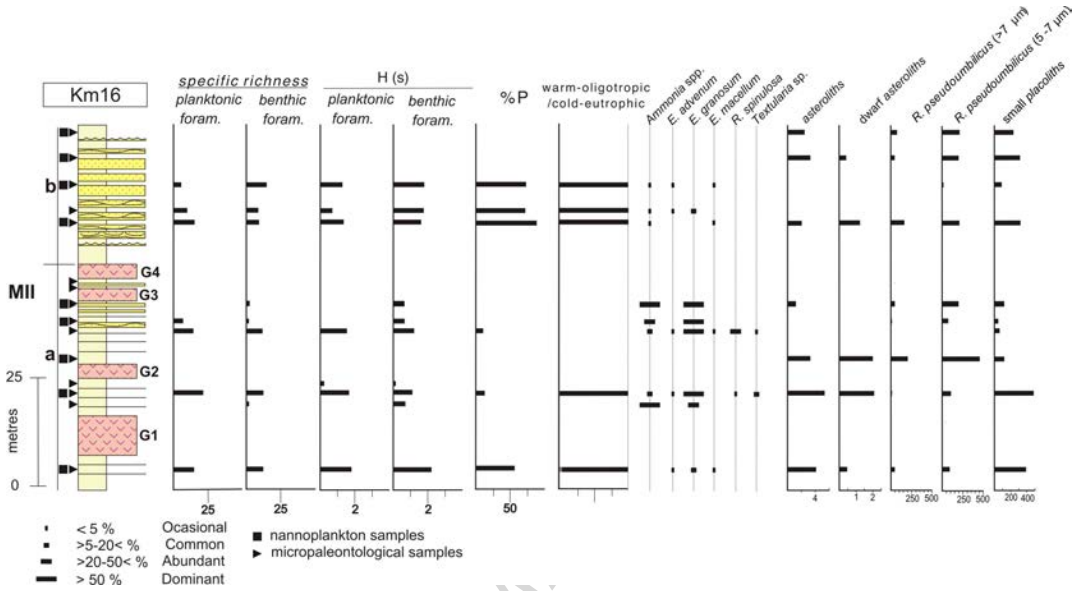

Figure 11

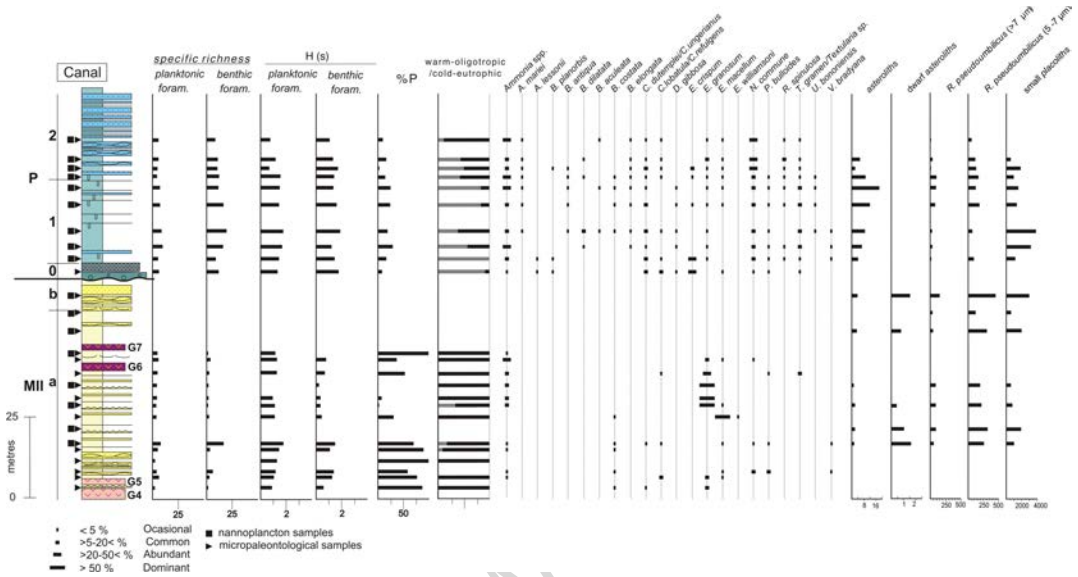

Figure 12